3B2v8.06a/w (Dec 5 2003).51c XML:ver:5.0.1 JQSR : 1459 Prod.Type:COM pp.1–23(col.fig.:1,3,4,6,7,8,9,10) ED:Sushma PAGN:NMN SCAN:Anil

ARTICLE IN PRESS

ELSEVIER

Quaternary Science Reviews ▮ (▮▮▮▮) ▮▮▮–▮▮▮

QSR

First appraisal to define prospective seismogenic sources from historical earthquake damages in southern Upper Rhine Graben

Umberto Fracassi[a,*], Bertrand Niviére[b], Thierry Winter[a]

[a]*Bureau de Recherches Géologiques et Miniéres, Div. ARN/MAS, B.P. 6009, F-45060 Orléans cedex 2, France*
[b]*UMR5831-Imagerie Géophysique, Université de Pau, BP 1155, F-64013 Pau Cedex, France*

Received 1 December 2002; accepted 26 May 2004

Abstract

The southern portion of the Upper Rhine Graben, a major oblique rift among France, Germany and Switzerland, shows a weak instrumental seismic record despite its remarkable physiographic imprint within the Northern Alpine foreland. Since traces of active deformation can be found in this region and based on experience in other European areas with high seismic hazard and dense population, we searched for past earthquakes recorded in historical catalogues. Based on the fact that tectonic deformation cumulates through geological time and considering that long-term effects tend to leave characteristic signatures on present-day landscape arrangement, our goal was to identify faults that could have caused the damage of recorded historical events.

We isolated five main earthquakes, of moderate Richter magnitude, essentially located on the E flank of the graben (as is the case with recent seismic activity). To such events, we were able to associate a specific prospective structure through the use of a procedure thus far successfully employed in Southern European contexts. We concentrated on three events which showed (a) notable sensitivity to the density of the historical felt reports and (b) accordance with on-going subtle deformation pattern. Another, most relevant earthquake (M 5.5) yielded a promising match with the known deformation network in the region.

As a template to better constrain earthquake cycle and damage potential, historical seismicity offers an invaluable tool, since it contains a specific record, although not always unambiguous. Cross-checking such data with pertinent geological information allows to devise a realistic fault geometry capable of being responsible for a specific seismic event.

1. Introduction

1.1. Detecting seismogenic sources from historical records

Overall seismicity patterns are a key tool to assess ongoing deformation mechanisms in tectonically active regions. Such patterns show up from recorded seismic event of the last 25–30 years, that is after the inception of permanent seismic networks. Nevertheless, to ascertain the recurrence time of a given earthquake and to search for a prospective fault potentially causative of an older event, a much longer timespan needs to be accounted for. To this purpose, historical catalogues contain a compilation of data describing past earthquakes.

Such non-instrumental coverage yields a precious wealth of information, together with some uncertainties (Musson, 1998; Albarello et al., 2001) which have to be taken into account. First of all, a catalogue only contains felt reports. These can be described as local and contemporary records of damages reported either as historical documents or private correspondence. Such documentation is then translated by present-day approaches into an objective evaluation of actual damages (sometimes below or beyond descriptions), expunging style of report and balancing the true authenticity of various documents that describe a recognizable location.

*Corresponding author. INGV, Via di Vigna Murata 605, I-00143 Roma, Italy. Tel.: +39-06-51860557; fax: +39-06-51860507.
E-mail address: fracassi@ingv.it (U. Fracassi).

0277-3791/$ - see front matter © 2004 Published by Elsevier Ltd.
doi:10.1016/j.quascirev.2004.05.009

The ultimate goal, clearly, is to then render the entire process into a single intensity value for a given locality.

As one moves back in time, languages, dialects, documents, hand drawings etc. all become less obvious. However, even in ideal situations, i.e. a readable and self-consistent dataset of records for a given date/event, compilation of damage isolines, needed to pin down an intensity pattern, remains a complex task. This is specifically due to two main facts: (a) local intensities in the catalog were derived from descriptive information and (b) identifying a precise location for a specific record may not be univocal. A typical example is our study region, which underwent different dominations across the centuries (a common feature in Europe; see Esposito et al., 1995; Lambert and Winter, this volume) and even hosted a local language (Alsatian), so that locality names were altered back and forth from one tongue to another. The result commonly caused placenames which have some shared traits in two similar dialects (and that could therefore be considered as a single locality) to eventually appear under two distinct sites—and possibly coordinates as well. On the other hand, since intensity values and geographical location of felt reports are the critical information in a historical catalogue, their reliability influences the overall assessment of a prospective seismogenic source.

Furthermore, while historical records contain a wealth of information, often not entirely exploited, they also inherit the material complexities needed to compile them. Most of the evaluation about the data reliability remains solely with the database curators, which are thence meant to convey data arising from felt reports and their descriptions into a coherent document (Boschi et al., 2000; Albarello et al., 2001). In this study, we merged the former input with geomorphological and geological data, augmented by seismic events from the instrumental era. This allowed us to infer potential seismogenic sources for the most prominent (epicentral intensity > VI MSK degree) historical earthquakes covering the last 1200 years. (Lambert et al., 1996) between the border fault systems that flank the S portion of the Upper Rhine Graben.

The background data set we employed for most maps, calculations and geomorphic evaluation is a Digital Elevation Model. It was obtained from the merger of the French source (courtesy of BRGM) at a nominal resolution of 50 m and the German one (courtesy of Universität Freiburg) with a 25 m posting. Although the country border corresponds to the Rhine river course, the German dataset actually covers a broad portion of interior French territory. This resulted into a merged database with a 25 m resolution for most of the research area.

1.2. Geological and geodynamic scenario of the Upper Rhine Graben

The Rhine Graben is an oblique rift (Ziegler, 1992), 300 km long and 40 km wide, from Mulhouse (France) to Frankfurt (Germany), trending SSW-NNE. As per its imprint in the geodynamic arrangement of Western Europe (Fig. 1), the rift basin is hosted within the Vosges Mountains to the W, the Black Forest to the E, the Rhenish Massif to the N and the Jura thrustbelt to

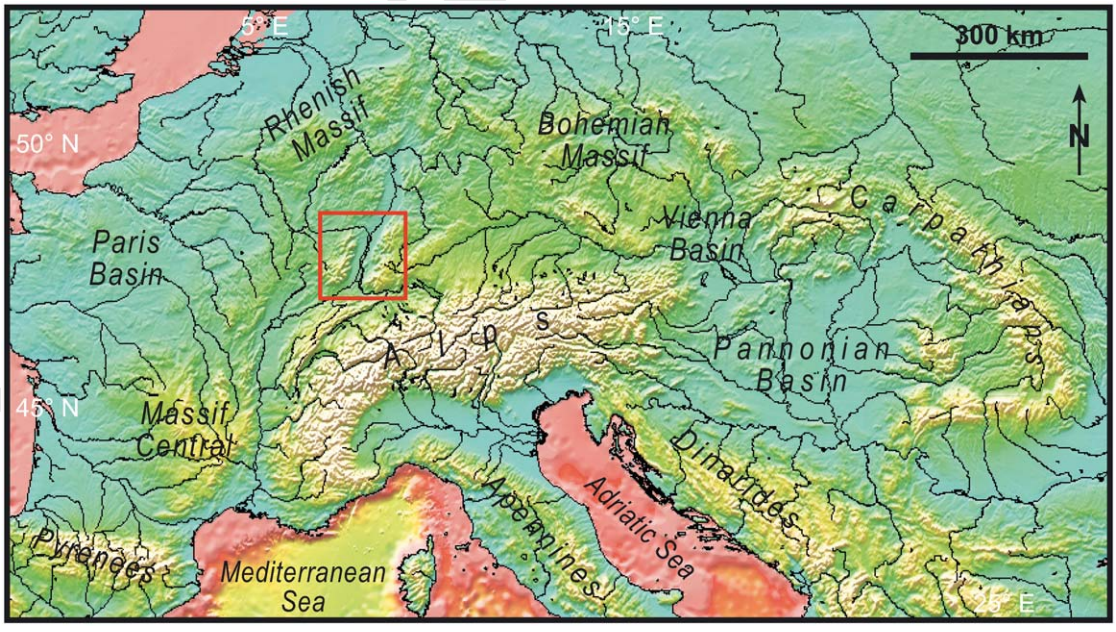

Fig. 1. Main regional elements of continental Europe and bounding basins, including the southern Upper Rhine Graben (in the red box) (*topographic data courtesy of Scripps Institution of Oceanography© 1987*).

the S (Becker, 2000). Together with the Vienna Basin, it is a prominent feature of the N Alpine Foreland (Illies and Greiner, 1978; Ziegler, 1992).

Its inception dates back to the Upper Eocene, starting with E–W extension (Bois, 1993), apparently in accordance with pre-existing weak zones (Bonjer et al., 1984; Clauser et al., 2002). From Eocene until Aquitanian time, the graben was mainly fed by shales and sandstones; extensive evaporites deposited in the S portion (Bois, 1993; Sissingh, 1998; Derer, 2003). Since the Middle Pliocene, the tensional graben twisted into a broader overall shear zone, predominated by a strike-slip kinematics (Ahorner, 1975) and by the typical 3D oblique rift arrangement (McClay et al., 2002). The graben cuts through the Lalaye–Lubine–Baden Baden crustal discontinuity, a remnant of the Variscan orogen; the accommodation zone of the Rhine Graben developed across this major oblique fracture system (Brun et al., 1992; Mayer et al., 1997).

The shape of the Oligocene depositional top indicates the quantitative difference in subsidence and its geometry along the Rhine Graben (Brun et al., 1992). Fig. 2a illustrates the present-day arrangement of the alluvial aprons with respect to the architecture of the graben shoulders. The majority of the depositionary framework developed on the W margin, with the course of the Rhine river that flanks the W rims of the above alluvial system. Brüstle (2002) discussed the evolving drainage directions that the Rhine followed since early Quaternary time and effectively pointed out how the river course repeatedly switched from W to E (and viceversa) of the Kaiserstuhl volcanic complex. Based on borehole data, this author postulated that the footwall of the Freiburg fault system (Behrmann et al., 2003) acted as a depositionary threshold for the local alluvial system originating from the Black Forest.

At the crustal level, Brun et al. (1992) explained the broad architecture of the graben. Figs. 2b and c show their interpretation of the geometry of the master faults N and S of the Lalaye–Lubine–Baden Baden Fault Zone. The former cross-section highlights the uplifted shoulder of the Bayern and its border fault now cross-cutting the upper crust. Conversely, the latter one shows an opposite scenario, where the Vosgian fault controls the creation of accommodation space in the SW portion of the basin, together with a number of synthetic systems. Such evidence suggests a depositionary system from the W margin essentially steady through Quaternary time, given the age of the terrains (Briquet, 1931). However, instrumental seismicity (although of $M_w \leqslant 3.0$) concentrates on the opposite shoulder (Fig. 2d), with hypocenters gradually deeper towards the Freiburg border fault, forming a sparse cloud of events in the 10–20 km depth region (Bonjer, 1997). This information will prove its relevance in the following chapters when we compare the overall earthquake distribution and occurrence with the landscape evolution in the Upper Rhine Graben.

1.3. Long-term vs. short-term indicators of recent activity

The former lines of evidence indicate a seeming seismotectonic inconsistency, in as much as a certain seismic activity on the SE shoulder of the Upper Rhine Graben identifies an ongoing deformation in the vicinity of the normal border fault. Conversely, the sedimentary pattern discussed by Menillet (1995) and depicted in Fig. 2a highlights a depositionary scenario predominated by sedimentation currently detectable only along the W margin, with a major river system flowing towards NE (Brüstle, 2002). Whatever present-day feeding from the Black Forest is either concealed by the Rhine thalweg, as borehole data indicate (Brüstle, 2002), or smoothed away towards N by the Rhine itself. The river's sweeping course likely competed with the vosgian alluvium, acting either as a mere E boundary to the fan system or trimming its distal aprons, as often described in other areas (Fracassi, 2001; Keller and Pinter, 2002). This view essentially conforms to the sedimentary model envisaged by Leeder and Gawthorpe (1987) for axial-through drainage in half-grabens.

To substantiate this physiographic scenario, we took into consideration the relationship between the Rhine and the Ill river, flowing in the W side of the graben. Differently from the Rhine, which is a major European drainage feature, the Ill is a minor, local tributary streaming from the Jura foothills up to Strasbourg, where it eventually joins the Rhine. Despite the outstanding difference between the two rivers in terms of transversal section, discharge and geomorphic role, their courses are remarkably parallel (Fig. 3a). This is particularly evident in three points where both rivers undergo sharp shifts in their flow. Both courses bend of $\sim 60^\circ$ to the W, approximately at the same point along their thalweg. The first W-ward shift is located immediately N of Mulhouse. It is then repeated towards N, this time close the Kaiserstuhl volcano. Should we assume that the latter, which certainly is a relevant landscape feature, did act as a geomorphic threshold for the Rhine (flowing immediately W of the Kaiserstuhl), it would be difficult to raise the same consideration for the Ill river, ca. 20 km to the W. Finally, a further E-ward shift, of similar entity to the previous ones, can be found near Rhinau.

Fig. 3b compares and contrasts the longitudinal profiles of the Rhine (red) and the Ill (blue) with the dip of the paleo-landsurface (green) acting as drainage divide between the two rivers. This surface plunges towards W (negative values) for most of its area, although noteworthy changes occur along-track. Such perturbations are essentially the W-wards peaks that occur where the rivers change flow directions. Most

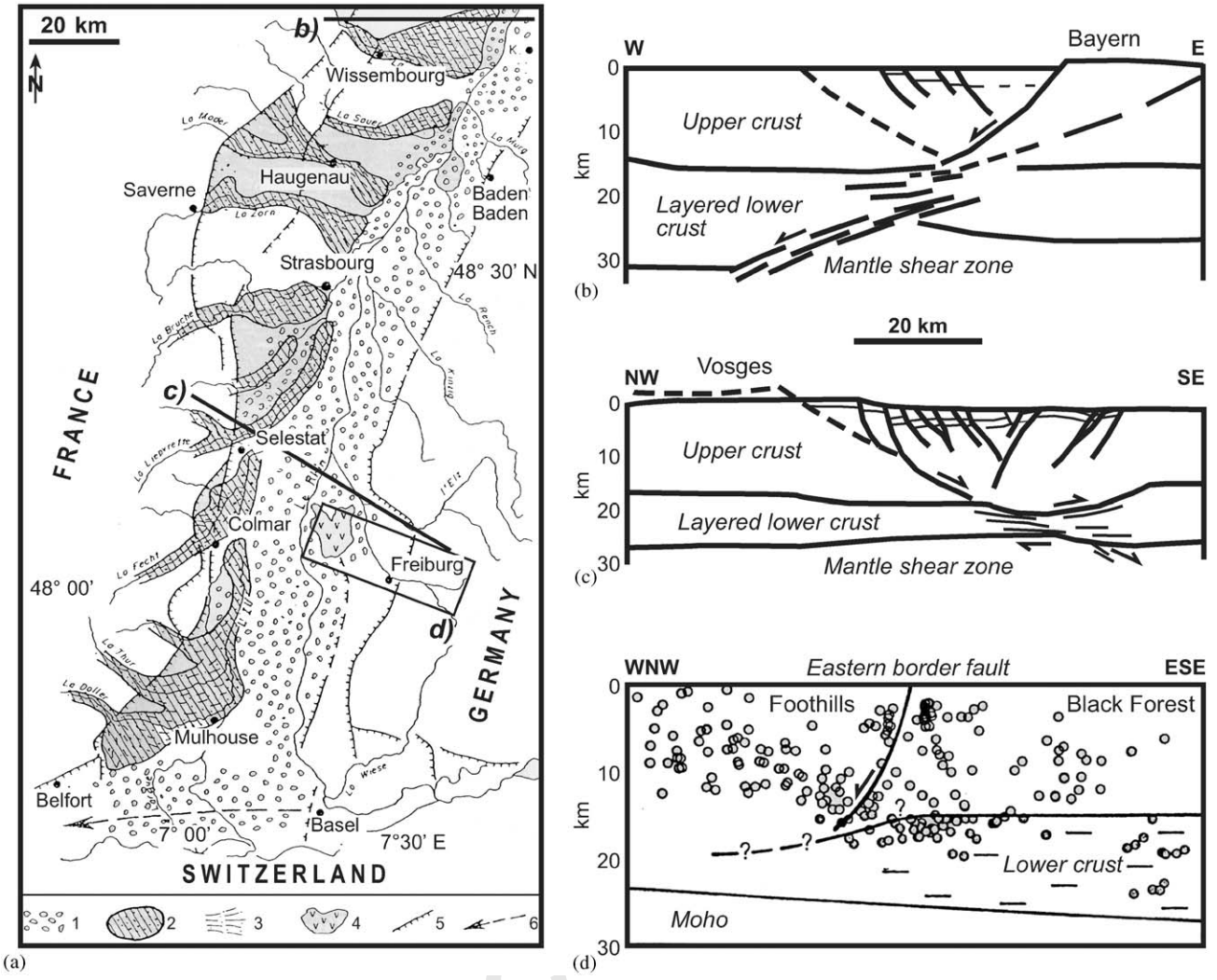

Fig. 2. (a) Generalized arrangement of alluvial systems from Mulhouse to Wissembourg (from: Menillet, 1995). The vast majority of fan deposition occurs and/or is currently detectable on the W border of the oblique rift. The Rhine flanks to the E the fan arrays. 1: Rhine alluvium; 2: Vosges alluvium; 3: vosgian rivers alluvium; 4: Kaiserstuhl volcano; 5: major border faults of the Upper Rhine Graben; 6: Rhine river flow direction during Upper Pliocene time. (b) and (c) Crustal cross sections of the ECORS-DEKORP deep seismic reflection campaign (approximate location on a), showing the vergence switch in the oblique rift N of Strasbourg (redrawn, from: Brun et al., 1992). (d) Projected occurrence of small seismic events ($M_w < 3.0$) recorded on the SE border of the Upper Rhine Graben (from: Bonjer, 1997).

interestingly, the longitudinal profiles of the Rhine and Ill show two remarkable peculiarities:

(1) the Rhine essentially flows at an higher elevation than the Ill. Such feature contrasts with (a) the general erosive efficacy ascribable to the Rhine and (b) its overall water and sediment load;
(2) the paleo-landsurface is not dipping towards the major drainage vector (the Rhine). While the Ill is not likely to exert a notable erosive role on present-day topography, we infer that a major, long-wave surface warping is controlled by the W master fault (as defined by the crustal seismic reflection data in Brun et al., 1992).

The geomorphological scenario illustrated in Fig. 2 and the recent and current landscape arrangement show that in the S Upper Rhine Graben fan deposition and creation of accommodation space predominantly occurred on the W border. This complies with the setup that would be expected from a physiographic standpoint and in accordance with accepted drainage models for half-graben evolution (Leeder and Gawthorpe, 1987). However, from Menillet (1995) and Brüstle (2002) we know that the Rhine consistently flew on the E flank of the graben, i.e. opposite to the W master detachment fault on the Vosgian foothills. Therefore, since river systems are the most sensible landscape indicators, ongoing geomorphic processes are not likely to be controlled by the fault system on the W flank, but are conceivably very recent or at their inception stage.

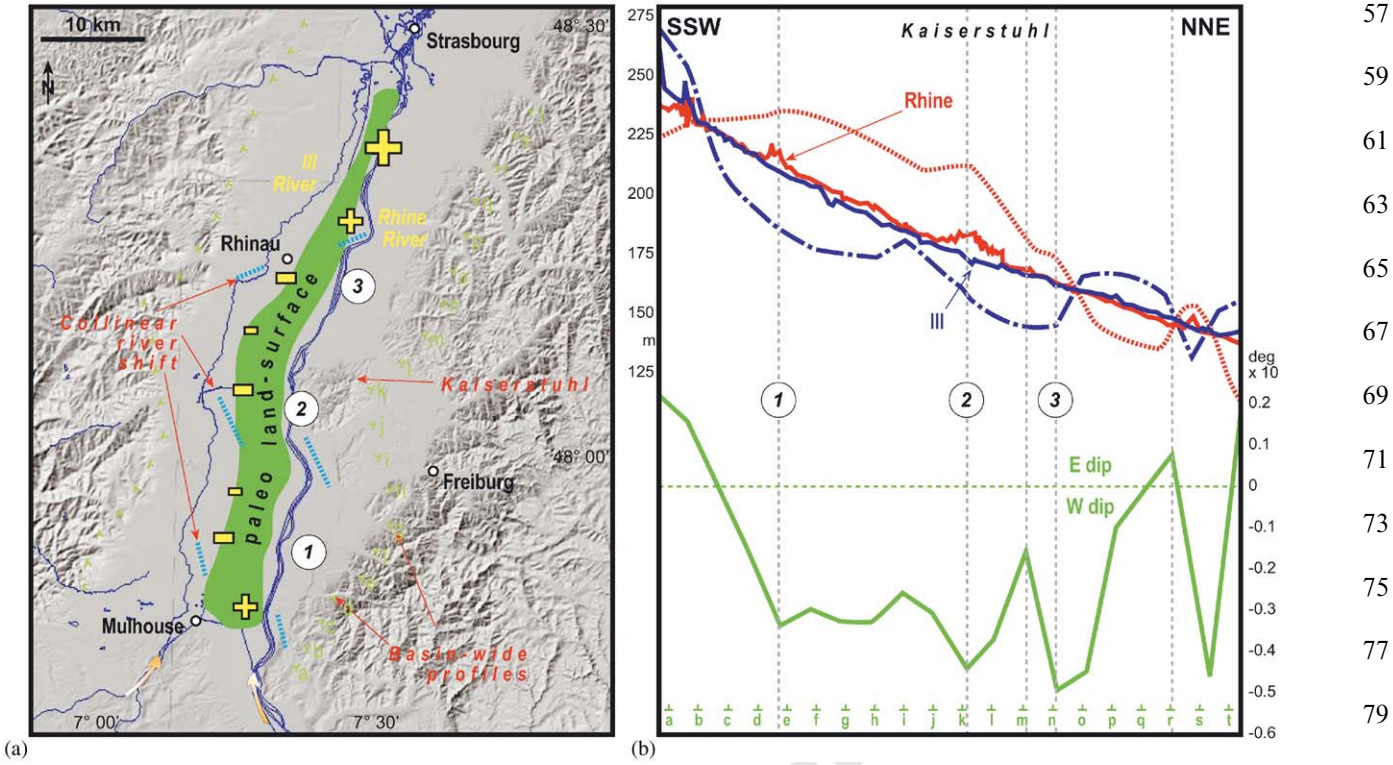

Fig. 3. Profiles of morphometric longitudinal signatures along thalweg of Ill (blue) and Rhine (red) rivers, from Mulhouse (Ill) and Basel (Rhine) in the S towards Strasbourg to the N, where the Ill joins the Rhine (a). Dotted and dashed-dotted lines are the amplified profiles (b). a-t are the transverse profiles of the paleosurface acting as a drainage divide between the two rivers. Notice the three peaks in the dip of the surface towards W corresponding to the three major shifts in the course of both rivers. Left scale of (b) is height of river thalweg (in m); left is dip of paleosurface (in degrees). "+" and "−" are dips towards E and W, respectively; larger symbols indicate higher dip values.

The seismic events recorded on the SE border of the graben yield magnitudes and depth of focal mechanism ($M < 3.0$ and depth well below 10 km; see Section 2.4) which seem difficult to fit the amount of energy needed to influence the landscape (Keller and Pinter, 2002). Moreover, seismicity is concentrated on the eastern margin of the graben and not on the western one, where deformation is plausibly expected from the geomorphic features. There is thus a discrepancy on the localization and the mechanisms of deformation between long-term and short-term activity. The former (concentrated on the western master detachment) is pinpointed by large wavelength depositional and geomorphic evidences, representative of few 10–100 kyrs, whereas short-term activity (centered upon the minor antithetic faults on the E boundary) is highlighted by clustered seismicity and short wavelength interferences on landscape (Brüstle, 2002). One possible explanation is that the era of instrumental seismic recording is too short to record past earthquakes that were capable of ground-warping and that occur at long recurrence times (Machette, 2000). This could be verified by searching evidences of past events in paleoseismological (Lemeille et al., 1999a, b) and/or historical records. However, another explanation is that the earthquakes on the E margin witness a short-term activity, which did not yet warp the surface, while the W border expresses the cumulative motion of stick-slip deformation (as per the definition of Brace and Byerlee, 1966) and is capable of altering the landscape within a much longer geomorphic timespan (Vogt, 1991; Hetzel et al., 2002). If either of the above scenarios apply, efforts need to be concentrated on the records of historical seismicity and on geological information from the subsurface.

In summary, the two options may well invoke consistent mechanisms, in as much as longer seismic cycles with larger (and possibly older) earthquakes could be associated to the western edge, while the eastern one is likely causative of local and continuous accommodation, yielding events with a much shorter recurrence time and consistently smaller magnitudes.

2. Earthquake database

2.1. The historical data set: availability and implications

This research stems from the exploitation of the felt reports for a number of earthquakes belonging to the pre-instrumental era. Due to its overall self-consistency

and the availability of felt reports, the main source of data was the French Catalog, SISFRANCE (2004), which already incorporates information from bordering countries about trans-frontier earthquakes. We performed cross checks on the main German Catalog, managed by Budesanstalt für Geowissenschaften und Rohstoffe (BGR), the regional one of Landesamt für Geologie, Rohstoffe und Bergbau Baden-Württemberg (LGRB) and the Earthquake Catalog of Switzerland (ECOS) held at the Eidgenossische Technische Hoschule Zürich (ETHZ). We also referred to previously published German data such as Sieberg (1940) and Leydecker (1986) and the 2003 German Quakecat online epicenter catalog.

We accessed the SISFRANCE© internal database for the south-central Upper Rhine Graben and its surroundings (47°45′–49°00′ N; 6°30′–8°30′ E). Since we were aiming at events that could have caused prospective ground warping, the minimum desired intensity was set at VI, with the ultimate goal of detecting events corresponding to a M_e (equivalent magnitude; Gasperini and Ferrari, 2000) of at least 5.0. This value is actually lower than 5.5, commonly associated in Southern Europe to viable seismogenic sources that can be (a) realistically recognized by means of geological tools and (b) responsible for inducing significant seismic risk (Valensise and Pantosti, 2001b; Carena et al., 2002; Valensise et al., 2002). However, we feel the 5.0 value to be more suited to the overall low seismicity of the studied region, thus suggesting that we should concentrate on the prospective cumulative effect of moderate earthquakes through geologic time (Loew et al., 1989; Keller and Pinter, 2002). The landscape perturbation issue is substantiated by previous and ongoing research trying to assess the tectonic relevance of suspectedly non-erosive scarps in the region (Vogt, 1992; Bano et al., 2000; Brüstle, 2002).

SISFRANCE© incorporates all localities for which a document or a citation was individuated. Among these localities, not all of them were originally associated to a MSK value or, in other cases, effects were felt but no actual damage was reported. Clearly, while the former case is of no sufficient information, the latter is of no usefulness as well. Therefore, we could not comment on damage for which a value could not be estimated, although in more that one case, "blank" localities (none or unknown damage) were close to others bearing a V or VI. Such geographical proximity, however, could not be the basis to infer or assume damage of an entity similar to close locations for which a MSK value was known. Thus, we chose to omit all localities for which there is no clear evaluation of the damage, even when they were located well within the subsequent damage pattern.

A total of 28 events reported I_E (epicentral intensity) of at least VI in the MSK macroseismic scale (as defined in: Grünthal, 1998). For each earthquake, the catalogue includes a list of the felt reports. Out of the above 28 results (Fig. 4), only 14 are based on reports sufficient to compute a seismogenic source, with only 11 earthquakes from the Upper Rhine Graben itself. Of these, only 6 returned a $M_e > 5.0$, including the largest ($M_e = 6.44$), represented by the well known Basel event of 18/10/1356 (Ahorner, 1975; Meyer et al., 1994; Lemeille et al., 1999a, b; Meghraoui et al., 2001; Lambert and Winter, this volume). However, while the remaining five were placed within the graben, the Basel earthquake entails a fairly more complex tectonic scenario, given its position across the Jura front and the switch between the compressive regime N of the Alps and the transtensional system in the graben itself (Niviére et al., 2003; Niviére and Winter, 2001; Winter et al., 2002). Therefore, we decided to concentrate on the five solutions as above, while the Basel event forms part of a larger on-going study.

Fig. 4 illustrates the locations of both historical (Table 1) and instrumental (Table 2) events considered. Concerning the first ones, earthquakes were chosen for epicentral intensity (I_E) > VI MSK (green-rimmed circles). However, I_E never exceeds VII, underlining the fact that current catalogs did not record catastrophic earthquakes (but for the Basel one). Historical events were most frequent N of Strasbourg across the Lalaye–Lubine–Baden Baden Fault Zone, highlighting the central sector of the SW–NE transfer zone in the graben. Another large group of events occurs in the vicinity of the Kaiserstuhl complex and near the Freiburg border fault, thus witnessing a degree of activity on the SE flank of the graben. Further earthquakes are located close to the Swiss border and the Jura Front, including the major one occurred in Basel. No events with I_E > VI occurred on the SW border of the graben (Table 3).

Most of the instrumental earthquakes were recorded well Freiburg and S of Mulhouse. Most focal mechanisms yield strike-slip and oblique-normal solutions (in accordance with known stress field; Ahorner, 1975; Schumacher, 2002), particularly NE of Freiburg and N of the Kaiserstuhl. The deepest hypocenters concentrate between Freiburg and the inner Black Forest, with the lowest M_w values.

As earlier pointed out, historical seismicity above the damage threshold is virtually absent from the SW flank of the graben and only five events could be associated to a significant magnitude (> 5.0), while instrumental ones rarely exceed M_w 3.0. With respect to the frequency-magnitude relationship, Ahorner (1975) indicates relatively low b-values (0.71) for the Upper Rhine Graben, especially if compared to 0.84 for the Lower Rhine Graben, N of our study area. This reflects the difference in maximum magnitude that can be deduced from the entire (historical and instrumental) seismic record in the former ($M = 5.5$) and latter region ($M = 6.0$), although

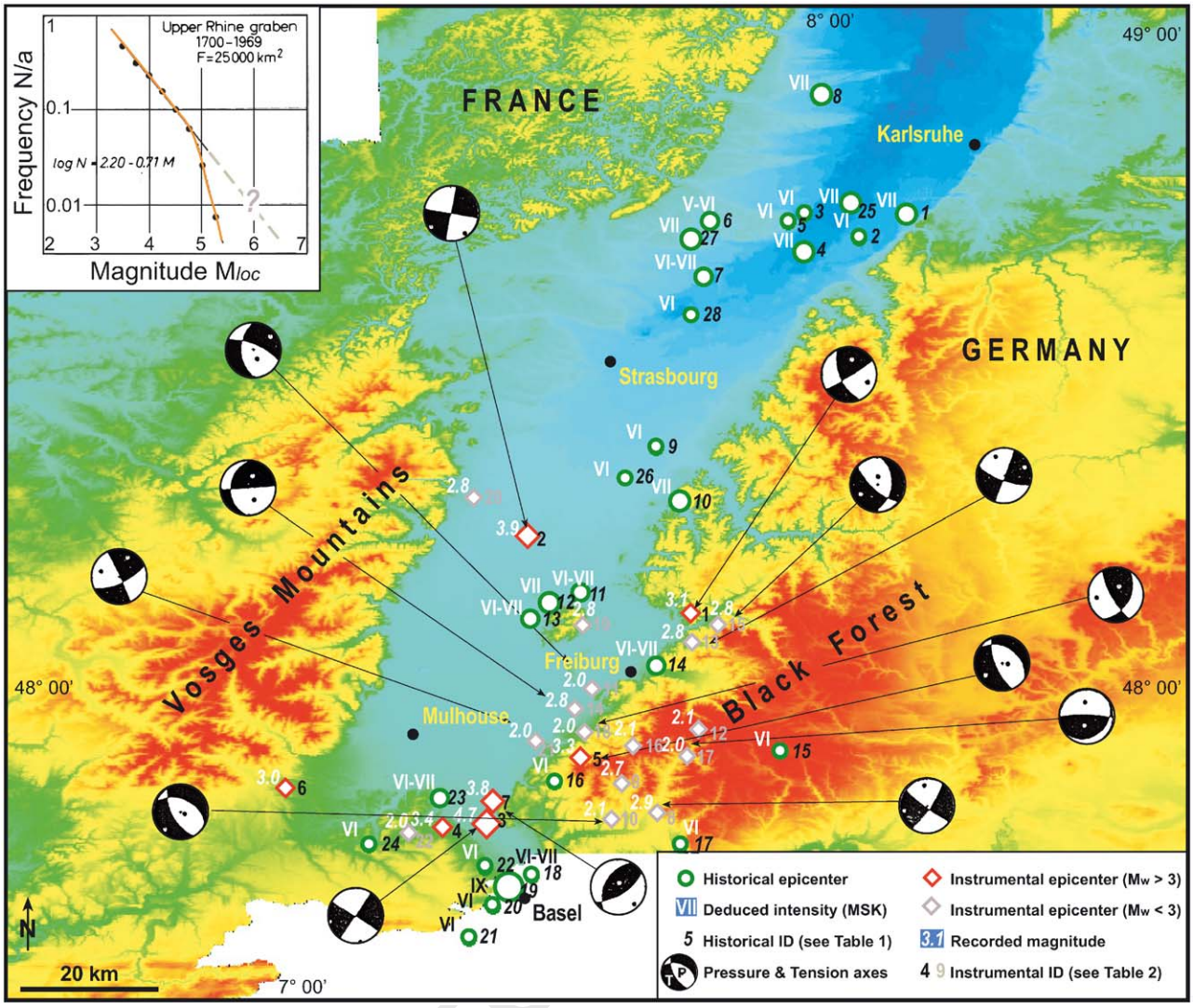

Fig. 4. Location of all main historical (see Table 1) and instrumental (see Table 2) seismic events in the south-central Upper Rhine Graben selected for this research. Top-left inset: *b*-value estimates for the Lower (top) and Upper (bottom) Rhine Graben (from: Ahorner, 1975). Thick grey dashed line is a potential projection of the linear relationship if (more) larger events were not recorded by available catalogs, due to hypothetically very long recurrence times. Events were selected on the ground of $2.0 < M_w < 3.0$ (grey-rimmed diamonds) and $M_w > 3.0$ (red-rimmed diamonds). Source mechanisms, as calculated by Bonjer (1997), are available for a portion of the mapped earthquakes.

still parts of the same geodynamic province. However, due to the fact that only five earthquakes show a magnitude above 5.0, calculations by Ahorner (1975) show that a linear relationship for the Upper Rhine Graben cannot fit the magnitude classes (inset in Fig. 4). Most earthquakes are of small magnitude and fit only a partial *b*-value up to the threshold of $M = 5.0$, above which the very few events we discuss in this work occurred. Almost all earthquakes in the Upper Rhine Graben, including the low magnitude instrumental ones and the historical ones with $I_E > \text{VI}$, are found on the E border.

The absence of earthquakes in the overall record on the SW edge of the graben can be due to at least two causes. One, if less conservative, is that the W master detachment provokes large magnitude events at comparably very long recurrence times, i.e. well above the currently available historical and paleoseismological record. In other words, the curve that would fit Ahorner's (1975) data cannot adequately take into account events that we do not know in the Upper Rhine Graben. In the hypothesis that more moderate (or catastrophic, i.e. $M \geqslant 6.5$) earthquakes would occur and/or be recognized in the future by other tools (i.e., paleoseismology), the *b*-value fit would be projected following the thick grey dashed line in the inset of Fig. 4. Since no such events are known, however, we cannot argue whether this area is capable of yielding a characteristic earthquake (as per definitions by: Schwartz and Coppersmith, 1984; López–Ruiz et al., 2004) with a very long recurrence time on the SW flank.

Table 1
List of historical seismic events of epicentral intensity > VI recorded in the south-central Upper Rhine Graben

	ID	Date	Time	Lat°,dd	Lon°,dd	NFR	RI_{loc}	I_{MSK}	RI_{MSK}	D_C	RD_C	Location
1	1120046	1356/10/18	22.00	47.517	7.550	54	B	9	K			Jura–Basel (CH)
2	1110007	1523/12/27	23.55	48.000	7.867		D	6.5	C			Black Forest–Freiburg (D)
3	1120053	1650/09/21	3.00	47.550	7.600		D	6.5	B			Jura–Basel (CH)
4	670020	1669/10/10	12.45	48.583	7.750		D	6	C			Plain de Basse-Alsace–Strasbourg (F)
5	670024	1728/08/03	16.30	48.350	7.917	30	B	7	B			Rhine Valley–Lahr (D)
				48.830	8.220					16	?	Rastatt (D)[a]
6	1110037	1737//05/18	22.00	48.917	8.300		D	7	B			Rhine Valley–Karlsruhe-Rastatt (D)
7	1110029	1737/05/11	15.00	48.917	8.300		D	6	B			Rhine Valley–Karlsruhe-Rastatt (D)
8	670139	1763/09/04	11.00	48.967	8.183		D	6	B			Outre Foret–Lauterbourg (F)
9	680031	1784/11/29	22.10	47.617	7.250		B	6	C			Sundgau–Altkirch ? (F)
10	1110214	1812/07/17	4.00	47.750	7.650		D	6	B			Black Forest–Kandern (D)
11	1110045	1823/11/21	21.30	48.150	7.700		D	6.5	B			Rhine Valley–Kaiserstuhl (D)
12	1120073	1836/11/05	7.00	47.483	7.517		D	6	C			Jura–Basel (CH)
13	1110054	1886/10/09	18.10	48.467	7.867		B	6	B			Rhine Valley–Offenburg (D)
14	1110056	1887/09/28	18.35	48.950	8.150		D	6	B			Rhine Valley–Karlsruhe-Rastatt (D)
15	1110013	1899/02/14	16.58	48.100	7.600		A	6.5	B			Rhine Valley–Kaiserstuhl (D)
16	680065	1901/05/22	7.57	47.567	7.500		A	6	A			Plain de Haute-Alsace–St. Louis (F)
17	1120077	1910/05/26	7.12	47.417	7.467		A	6	B			Jura–Laufen (CH)
18	1110017	1926/06/28	22.40	48.133	7.633	545	B	7	B	10	C	Rhine Valley–Kaiserstuhl (D)[b]
				48.130	7.680					8		[c]
19	1110069	1933/02/08	7.07	48.883	8.183	446	B	7	A	15	C	Rhine Valley–Karlsruhe-Rastatt (D)[b]
				48.850	8.200					6		[c]
										4		[d]
20	1110076	1935/12/30	3.36	49.217	8.217	678	C	7	K			Rhine Valley–Offenburg (D)[b]
				48.610	8.210		D			15	C	
21	1110083	1948/06/07	7.15	48.967	8.400		A	7	B			Rhine Valley–Karlsruhe (D)
22	670096	1952/09/29	16.45	48.833	7.967		B	6.5	B			Outre Foret–Wissenbourg (F)
23	670098	1952/10/06	22.27	48.950	7.983		D	5.5	B			Outre Foret–Wissenbourg (F)
24	670102	1952/10/08	5.17	48.950	7.983	51	A	7	A	10	B	Outre Foret–Wissenbourg (F)[b]
				48.900	7.966					7		Seltz (F)[a]
25	670106	1959/09/04	8.36	48.350	7.633		A	6	A			Plain de Basse-Alsace–Erstein (F)
26	1110021	1965/09/19	8.10	47.817	8.133		D	6	C			Black Forest–St. Blasien (D)
27	1110022	1974/05/21	7.42	47.617	7.917		D	6	C			Black Forest–Wehr (D)
28	680091	1980/07/15	12.17	47.717	7.400		A	6.5	B			Plain de Haute-Alsace–Habscheim (F)

IDs are unique identifiers to be found in the French Catalogue. Coordinates refer to ellipsoid International 1909 and datum European 1950. NFR = number of usable felt reports for the major earthquakes; RI_{LOC} = reliability index for location; I_{MSK} = felt intensity (transformed into numerical values: i.e., VI/VII = 6.5); RI_{MSK} = reliability index for intensity; D_C = focal depth computed by catalog compilers; RD_C = reliability index for focal depth (where available). Data courtesy of Jerome Lambert (BRGM) and SISFRANCE© (BRGM–EDF–IPSN). Computed focal depths and alternative epicenters are from:
[a] Leydecker (1986, 2003),
[b] Levret et al. (1994),
[c] Ahorner et al. (1970) and
[d] Ahorner (1975).

On the other hand, we still know that visible active deformation is actually found on the SW border; also, cumulative displacement on this side of the graben is witnessed by the basin architecture (Bartz, 1974; Brun et al., 1992). In a more conservative view, therefore, if we assume that the data set analyzed by Ahorner (1975) is a sufficient representative of the overall seismicity in this area, it could be possible that most seismic moment in the Upper Rhine Graben is simply released through smaller events ($M < 5.0$). The scarce occurrence of moderate earthquakes could then suggest that this part of the graben is not prone to accumulate sufficient seismic energy that would be steadily released through a number of events consistent with the projected *b*-value shown by Ahorner (1975). Since the cumulative small ($M < 5.0$) seismicity to-date available concentrates in the S Upper Rhine Graben (i.e., S of the Lalaye–Lubine–-Baden Baden system) while fewer but stronger events occur in the Northern portion, we tend to believe that smaller to (few) moderate earthquakes accommodate the accumulation of seismic energy in the studied area.

2.2. Computing the seismogenic sources

To appraise a prospective source from an array of felt reports, a number of parameters need to be computed, including distance of intensity points from the computed epicenter (Gruppo di Lavoro CPTI, 1999), attenuation

Table 2
List of instrumental seismic events of epicentral intensity recorded since 1974 in the southern Upper Rhine Graben. (a) include values so that $2.0 < M_w < 3.0$; (b) include values for $M_w > 3.0$

	Locality	Date	Time	Lat°,dd	Lon°,dd	Azim. 1	Dip 1	Azim. 2	Dip 2	M_w	Depth	Rake	Kinematics
(a)													
1	Waldkirch	1979/01/27	8.58	48.113	7.934	62	82	156	53	3.1	10.8	142.9	SS
2	Rhinau	1979/10/27	14.58	48.290	7.650	102	80	192	90	3.9	7	179.9	SS
3	Sierentz	1980/07/15	12.17	47.672	7.470	125	80	216	84	4.7	11.4	10.1	SS
4	Sierentz	1985/02/28	21.33	47.656	7.410	195	82	292	49	3.4	11.1	319	SS
5	Badenweiller	1988/08/26	0.30	47.804	7.688	158	65	307	30	3.3	19.4	284.8	NF
6	Belfort	1988/09/03	15.09	47.746	7.062	130	65	224	82	3	6.6		SS
7	Mulhouse	1980/07/16	15.00	47.681	7.486	54	53			3.8	12.1	110.6	TF
(b)													
8	Wiesental	1982/10/04	4.06	47.672	7.852	36	74	128	84	2.9	22.8	354	SS
9	Wies	1984/06/16	6.43	47.750	7.800	150	5	8	41	2.7	9.4	292	NF
10	Schopfheim	1985/08/13	2.17	47.680	7.776	315	55	90	44	2.1	18.8		NF
11	Munzingen	1985/09/15	18.18	47.954	7.733	180	44	295	68	2	13.5	327	NS
12	Todnau	1986/07/10	22.23	47.860	7.953	148	52	297	42	2.1	18.5	290	NF
13	Glottertal	1989/03/11	21.24	48.043	7.944	21	89	111	68	2.8	12.9	338.2	SS
14	Bad Krotzingen	1989/03/18	14.26	47.909	7.698	88	87	184	27	2.8	14	6.7	ND
15	Waldkirch	1989/04/07	6.36	48.086	7.980	7	36	132	68	2.8	15.1	319.3	NF
16	Belchen	1989/08/24	10.42	47.822	7.807	171	65	271	69	2.1	19.3		SS
17	Utzenfeld	1990/05/11	6.29	47.808	7.924	273	78	58	15	2	20.4	55.9	TF
18	Sulzburg	1990/06/20	10.59	47.848	7.713	31	35	151	71	2	17.4	144.8	TF
19	Kaiserstuhl	1990/09/14	2.14	48.100	7.662	186	60	279	84	2	7.8		SS
20	Selestat	1990/09/30	2.40	48.349	7.482	180	60	300	49	2.8	5.9		NF
21	Laufen	1991/01/01	7.29	47.836	7.654	336	87	68	64	2	11.9	333.4	SS
22	Mulhouse	1991/08/25	0.06	47.638	7.330	200	82	292	76	2	12.3	345.9	SS

Rake indicates slip direction with respect to N90°. NF = normal fault; TF = thrust fault; SS = strike-slip; ND = normal dextral; NS = normal sinistral. Coordinates are conformal to ellipsoid International 1909 and datum European 1950 (recompiled and modified, data after: Bonjer, 1997; Plenefisch and Bonjer, 1997).

Table 3
Format of input felt reports for the Kaiserstuhl 1926 event

11 DI 1926 6 28 22 40 Kaiserstuhl SISF 544 80 80 48 6,75 A 622 38 540 28 M 569 22 48 50043

48.10	7.33	5.5	MARCKOLSHEIM	682730001
48.12	7.19	5.5	RIBEAUVILLE	682570001
48.11	7.31	5.5	OHNENHEIM	681370001
48.35	7.49	5.5	KEHL	680520001
47.34	7.11	5.5	LARGITZEN	683370001
48.08	7.10	5.5	ORBEY	682470001
48.15	7.11	5.5	SAINTE-MARIE-AUX-MINES	680890001
48.07	7.29	5.5	JEBSHEIM	682620001
48.11	7.34	6.0	BOOTZHEIM	682920001
48.02	7.36	6.0	BREISACH	683480001
48.21	7.52	6.0	LAHR	682600001
48.03	7.41	6.0	WASENWEILER	683430001
48.00	7.52	6.0	FREIBURG	682910001
48.03	7.39	6.0	IHRINGEN	680820001
48.21	**6.41**	**6.0**	**BRU**	**683640001**
48.08	7.27	6.0	RIEDWIHR	682290001
48.01	7.32	6.0	NEUF-BRISACH	681880001
48.04	7.29	6.0	WIDENSOHLEN	682770001
48.06	7.33	6.0	BALTZENHEIM	680230001
48.08	7.37	7.0	SASBACH	682090001
48.09	7.44	7.0	RIEGEL	680260001

Bold indicates the Bru location, eventually expunged from the chosen solution.

laws describing intensity decay (Esposito et al., 1992) and aspect ratio for fault planes (Wells and Coppersmith, 1994). To this purpose, Gasperini et al. (1999) and Valensise and Pantosti (2001a) assembled the above algorithms into a single command-line tool, referred to as the Boxer© code. This program individuates the surface projection of a likely seismogenic source for the macroseismic field supplied by the user. The box, therefore, is the imprint of the fault according to the computed length, width and azimuth. Fig. 5 indicates the operational strategy within the software; for in-depth details of how Boxer© works, we provide an explanation in Appendix A (see: Gasperini et al., 1999; Valensise and Pantosti, 2001a).

Since there is a plausible lower limit to the dimensions of a fault to be considered as a potential source for a destructive earthquake (Kanamori and Anderson, 1975; Wells and Coppersmith, 1994), we focused on the seismic events for which one or more of the following factors were well constrained:

(a) M_e sufficiently above 5.0 (the higher the magnitude, the larger the prospective source and its potential

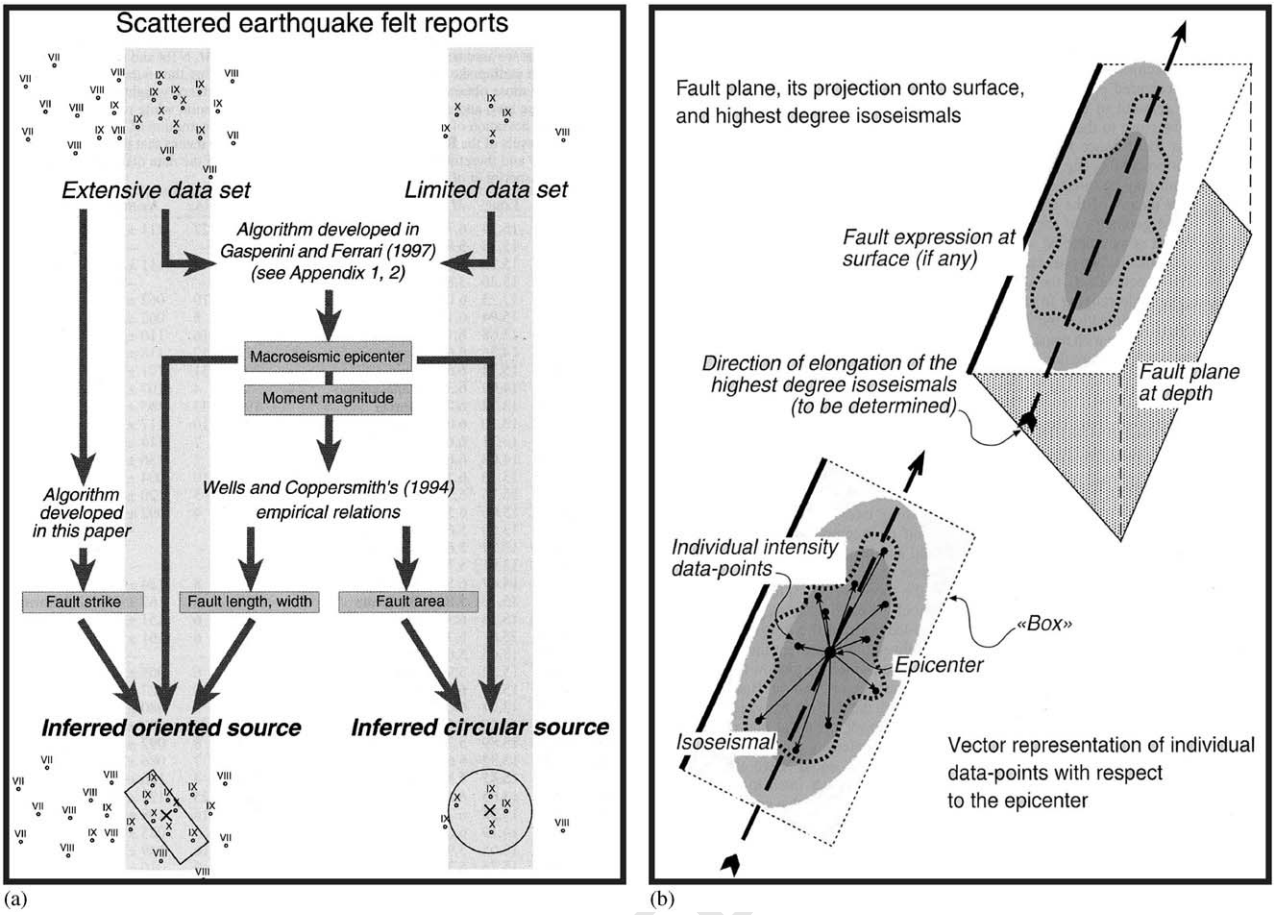

Fig. 5. Functional criteria of the Boxer© code. (a) Relationship between the sparse felt reports and geometrically inferred fault projection. (b) Geometry of the computed seismogenic source (from: Gasperini et al., 1999).

capability to interfere with the landscape through coseismic deformation);

(b) position (to best infer the likelihood of a structure and its geological relevance):
   b1—with respect to the known fault pattern and/or
   b2—by relevance with features of the graben, i.e. border fault, transfer systems;

(c) degree of knowledge and amount/intensity of felt reports in the earthquake data set.

Concerning the depth of the earthquakes we studied in detail, we notice that Ahorner et al. (1970) and Leydecker (1986) indicate various values, while other ones were estimated by Levret et al. (1994). Leydecker (1986 and 2003) also computed depths for earthquakes dating back to the Middle Ages. In the past, some authors (Kovesligethy, 1907; Blake, 1941; Sponheuer, 1960; Shebalin, 1973) devised algorithms to infer a plausible focal depth based on distance of a given intensity point from epicenter, isoseismal differences and variable attenuation parameters. Nevertheless, the above procedures are not common practice in the literature, since they tend to provide with very variable results, not always easy to constrain and/or compatible with previously known seismotectonic scenarios of investigated areas. Moreover, these empirical functions were originally thought and tested on several large earthquakes reported by a sizable number of high intensities (Blake, 1941), while such conditions are not to be found in the Upper Rhine Graben, where actually the structural and stratigraphic arrangement may also exert site effects on the intensity distribution.

Therefore, we preferred to keep a conservative approach towards estimated focal depths, while we favored the overall isoseismal arrangement with respect to the known geology and conceivable structure.

2.3. Virtues and vices of the historical events

As outlined in 2.1, only a minor portion of all available earthquakes with a $I_0 > \mathrm{VI}$ could be employed. This was due to the overall low intensities of the felt reports for most events, which prevented Boxer© to meet the condition $M_e > 5.0$.

With respect to location and intensities, an issue about data resolution needs to be raised. RI_{loc} and RI_{MSK} (see Table 1) represent the uncertainty factors for location and intensity, respectively. Concerning locations, A indicates the most reliable value (positional error within 5 km), while *E* yields an error > 50 km. As per RI_{MSK}, A indicates intensity error ≈ 0, while *C* refers to uncertain and/or sparse data clusters. *K* implies sufficient intensity reliability based on Sponheuer's attenuation law (Lambert et al., 1996). In line of principle, we found that the target final value of the most reliable felt report should comply, among other factors, with the following ones:

$$I_F = f(L_k \cdot I_k \cdot FR),$$

where I_F is the final (screened and filtered) intensity for a given locality, f is a devised and weighted function, L_k is a reliability factor for location, I_k is the reliability factor for intensities and FR represent the felt report value delivered by the macroseismic catalog. Reliability codes (in Sisfrance: from *A* to *E*) can be translated into numerical factors, so that $A = 1.0$ (thus unaffecting I_F), $B = 0.9$ and so on. In general, we found that I_k is inversely proportional to the probability that I_F is either under- or overestimated. Actually, a low I_k indicates a poor resolution of the provided intensity value; this statement, if realistic, does not necessarily imply a lower MSK neighbor for I_F. However, based on discrepancies commonly observed in felt reports across various earthquakes (Esposito et al., 1988; Lambert et al., 1996; Gasperini et al., 1999; Gasperini and Valensise, 2000; Stirling et al., 2002) and considering the degree of uncertainty in assessing felt reports merely arising from historical records, we can postulate that lower I_k's generally lead to smaller intensity values.

Finally, it is worth underlining that Boxer© was originally devised for the extensive Italian catalogs (spanning from 461 B.C. to 1992 A.D.) and the numerous moderate to large earthquakes ($M > 6.0$) therein. This implies that altering the attenuation factors in the algorithm would require a considerable number of equally suitable events. Conversely, the geodynamic scenario in our study area yields a rather different seismic record and overall magnitudes, both historical and instrumental. On the ground of these considerations, we chose not to amend the parameters, since we felt that any such customization would have been neither statistically constrained nor numerically consistent with the spirit of the Boxer© code and the groundwork behind it.

2.4. Constraints of the instrumental events

As earlier illustrated, only a fraction of all the available earthquakes with a $I_0 > VI$ could be employed in this research. In order to compare modeling results, we also selected instrumental events (Table 2). In several cases, fault plane solutions are in promising accordance with the known fault pattern described by Behrmann et al. (2003). However, apart from very few events, almost all instrumental earthquakes (Bonjer, 1997; Plenefisch and Bonjer, 1997) yield a maximum M_w below 4.0. Most events show $M_w < 2.0$, and are essentially deep (down to 20+ km). Such earthquakes are difficult to match the sources we obtained through Boxer©. Also, these events, with very small magnitude and at such depths, are not likely to add much constraint to the sources computed for historical events. Finally, the kinematics invoked by the fault plane solutions may be non-critical if extrapolated towards the surface (within the upper 10 km), where all our sources are possibly located.

3. Prospective seismogenic sources

3.1. Modeling isoseismal fields and coseismic deformation

To complement the calculations obtained through Boxer©, we associated information about the seismogenic box with the displacement field that a prospective source would cause if activated with a given geometry and magnitude. This was particularly true for the Lahr 1728 event, the earthquake with the highest magnitude (M_e 5.5) we deal with in this research.

In Appendixes 2 and 3 we explain in detail the procedures we followed. Concerning the macroseismic data, here we recall that, since felt reports are scattered points and are not necessarily showing a straightforward geometrical arrangement, we interpolated (using Carlson and Foley's 1991 algorithms) the intensity points to approximate a damage field and describe the resulting isoseismals. These were compared with the actual distribution of the original data points as per their location (i.e., whether on lowland or high relief or basin fill etc.), their clustering with other intensity data and the prospective seismogenic source.

As per the displacement or ground-warping prospectively caused by the earthquakes we studied, we tested the possibility that faults within or bounding the basin could be seismogenic sources using potential coseismic deformation. The surface displacement field that is expected from the 3-D solution of classical dislocation models (Okada, 1985, 1992) was compared and contrasted with the main geomorphic features of the area. This was pursued under the assumption that:

(a) the geometric solutions indicated by the historical record are compatible with observable fault planes;
(b) the total displacement of the prospective sources is the results of cumulative stick-slip events over geological time.

3.2. Overall seismogenic scenario

From the selection we exerted onto the available historical dataset, eight solutions were found for the studied area but only five of them yielded a $M_e > 5.0$ (Fig. 6). The most prominent earthquake analyzed is the one reconstructed from the macroseismic data of the 03/08/1728 Lahr ($M_e = 5.5$), at the boundary above which earthquakes can be considered (a) of significant seismic risk (Valensise and Pantosti, 2001b) and (b) potentially caused by a fault recognizable with geological and geomorphologic tools.

For the Lahr event, we notice that Leydecker (1986, 2003) specifies an epicenter fairly distant (~50 km NNE) from the one mentioned in the French catalog. This is due to the fact that this author suggests Rastatt and not Lahr as the location with I_{MAX}. However, no felt reports are published in catalogs other than Sisfrance, while Sieberg (1940) lists 28 localities, mostly in Germany. Of these, this Author could associate only six ones to an intensity value (IV/V), two of which already mentioned in Sisfrance. Furthermore, the latter catalog lists a cluster of four german localities (including Lahr) bearing a VII intensity all within a 10 km radius from the epicenter indicated by Boxer, thus realistically constraining the solution we propose. Therefore, for almost all localities in this event, the only available intensity points are the ones provided by SISFRANCE, which (until a new French–German compilation is available) we adhere to. Given the above reasons, we believe that the inner consistency of the overall database guarantees a homogeneity across the various earth-

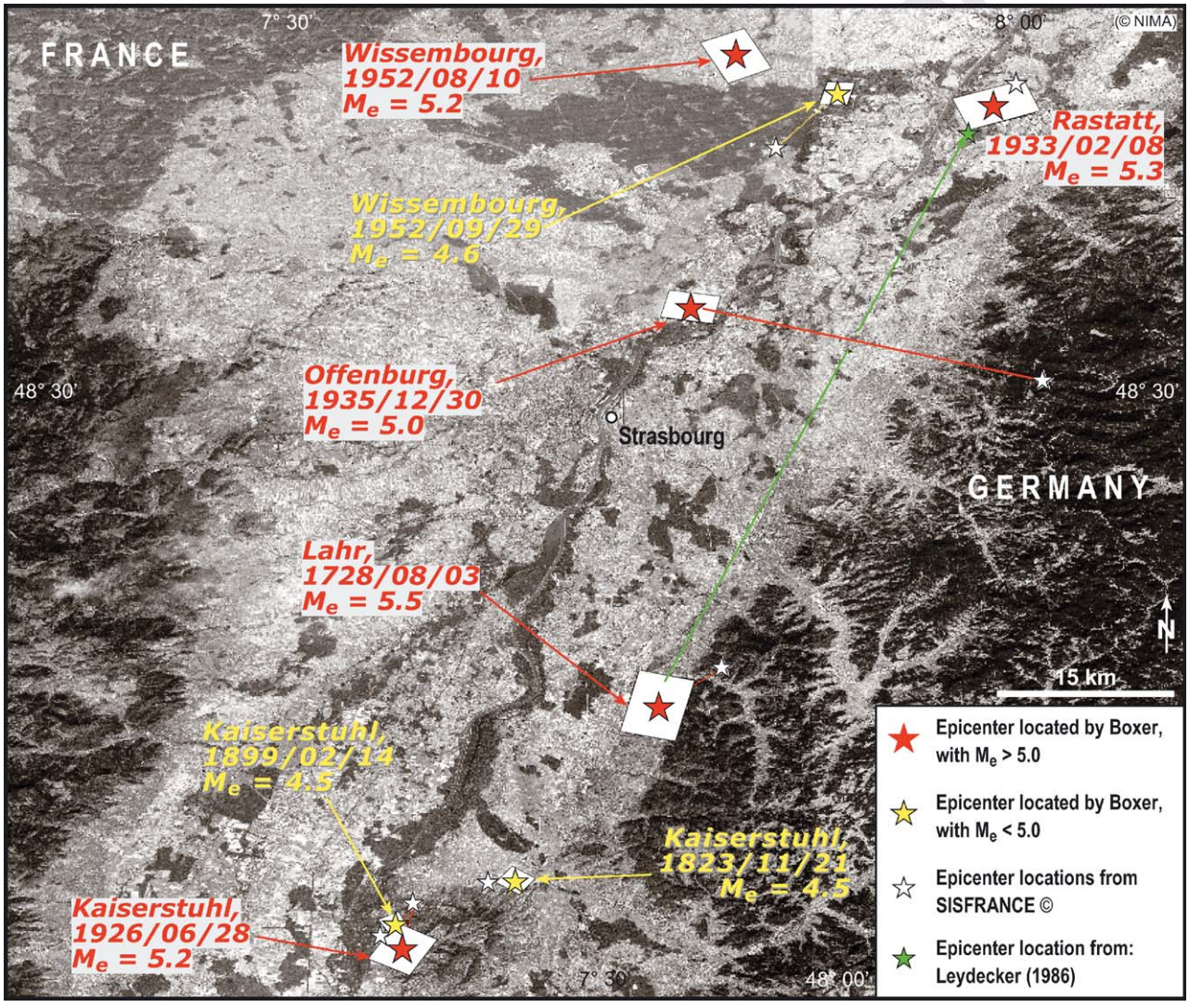

Fig. 6. Boxes of fault solutions, computed via Boxer, that yielded a $M_e > 5.0$ (in red). Other solutions were found for events with a sufficiently good coverage of felt reports, although the inferred M_e was <5.0 (in yellow). In some cases, the new epicenter, located by Boxer©, is remarkably distant from the one quoted in the historical catalogue (white star; see thin line linking with new epicenter). For the 1728 Lahr event, see also the epicenter by Leydecker (1986) displayed as a green star (*SPOT data courtesy of CNES/SPOT Image© 1992–1994*).

quakes, since historical felt reports were screened and compiled by a single team.

For the Offenburg 1935 event, we also notice that SISFRANCE presents an epicenter about 30 km E of the one calculated by Boxer. The maximum intensity points actually cluster in the upland across the German border E of Rastatt. The historical epicenter was reported between the VI values of Lautenbach and Forbach, with a distant VI in Karsruhe as well. We thus realize that:

(1) these values are clearly the highest in the macroseismic field for this earthquake and:
(2) SISFRANCE's epicenter is not a single isolated intensity point; rather, it appears to be well constrained by the amount of surrounding localities, of consistent intensities.

Therefore, we believe that the macroseismic information for this event is plausibly incomplete and feeds Boxer with data that are not entirely sufficient for a statistical analysis required by the code.

By magnitude-fault size relationships devised by Kanamori and Anderson (1975) and Wells and Coppersmith (1994), the computed boxes were normally about 4/5 km long and 5/6 km wide, apart from the Lahr case (6.2 length × 5.5 width). The latter and the 28/06/1926 Kaiserstuhl earthquakes are located very close to the Black Forest Border Fault and the Kaiserstuhl volcano. For this location, instrumental data indicate an event with azimuth compatible with the source we obtained, although M_w was much smaller.

Ordinarily, the epicenters computed by Boxer© are at small distance from the ones recorded in the SISFRANCE catalog. We should outline that, as in any such catalog, the historical epicenters were inferred from compilation of felt reports and were estimated from cross-checking accounts of various sources. Conversely, Boxer© re-establishes a statistical weighting of the overall reported macroseismic pattern and, particularly for the Lahr event, we feel that the relocated epicenters is more compatible with the geologic scenario. Concerning the Wissembourg 29/09/1952, $M_e = 4.6$ earthquake, the catalog's epicenter is equidistant from the new one and that of a previous event (of which this is a likely replica), that is Wissembourg 10/08/1952, $M_e = 5.2$.

3.3. Prospective sources vs. known structural pattern

To investigate their seismotectonic relevance, in Fig. 7 we plotted the five potential seismogenic sources together with solutions of recorded instrumental events onto the tectonic framework assembled by Behrmann et al. (2003). The overall fault pattern is dominated by brittle transfer zones, between Rhinau and Selestat, and few breached relay zones between Selestat and Strasbourg. The interconnecting splays reveal the fault branching typically found in oblique rifting (Chorowicz and Deffontaines, 1993; McClay et al., 2002). The major features are indeed represented by the E and W boundary fault systems (trending SSW-NNE) and the large accommodation zone running across Strasbourg, the aforementioned Lalaye–Lubine–Baden Baden system (striking SW–NE). This major hard linkage connects the E- and W-verging border faults (S and N of Strasbourg, respectively) shaping the half-grabens (as per Bartz, 1974) and their basement dip (after Brun et al., 1992).

As outlined in Table 2, most of the instrumental events show very deep hypocenters and low M_w. Although their seismotectonic input in this scenario is realistically limited (Carena et al., 2002; Miller, 2002) and mostly indicate a background seismic activity, a few solutions can be reasonably associated to major structures. Waldkirch 1979 (M_w 3.1) shows a fault plane solution in accordance with the sinistral slip along a ENE-striking strand of the E border fault N of Freiburg. Kaiserstuhl 1979 (M_w 2.9) provided a dextral solution comparable and adjacent to the box we computed for the 1926 (M_e 5.2) event and across the Rhine River Fault. Laufen 1991 (M_w 2.0) shows a mechanism compatible with dextral slip of a connecting splay NE of Mulhouse.

Concerning the historical earthquakes, the seismogenic boxes fairly well match the structural pattern, although, as said in 3.2, we opted to discard the solution for Offenburg 1935. This fit be seen explicitly for Lahr 1728, for which the proposed fault fits a structure previously recognized in Behrmann et al. (2003). This can be deemed also for Rastatt 1933, Kaiserstuhl 1926 and Wissembourg 1952, for which the inferred structures are compatible with the kinematic scenarios proposed in the literature (Schumacher, 2002 and references therein). The aforementioned Kaiserstuhl 1926, described in detail in 4.1, runs across the mean strike of the remnants of the volcanic complex. Wissembourg 1952 (M_e 5.2) crosses a hard rider W of Rastatt. Rastatt 1933 (M_e 5.3; see 4.2) is parallel to the accommodation zone NW of Baden Baden. The prominent Lahr 1728 (M_e 5.5; see 4.3) is possibly the most interesting event we detected, due to its magnitude and to its position essentially coincident with the eastern border fault between Rastatt and Freiburg.

We concentrated our interest onto the Kaiserstuhl 1926, Rastatt 1933 and Lahr 1728 events, due to their position with respect to the graben's features and their comparable magnitude and significant macroseismic framework. The first offers the largest record of felt reports, thus it was chosen as a best representative for the methodology discussed; the second is compared and contrasted with the former; the third case is the most

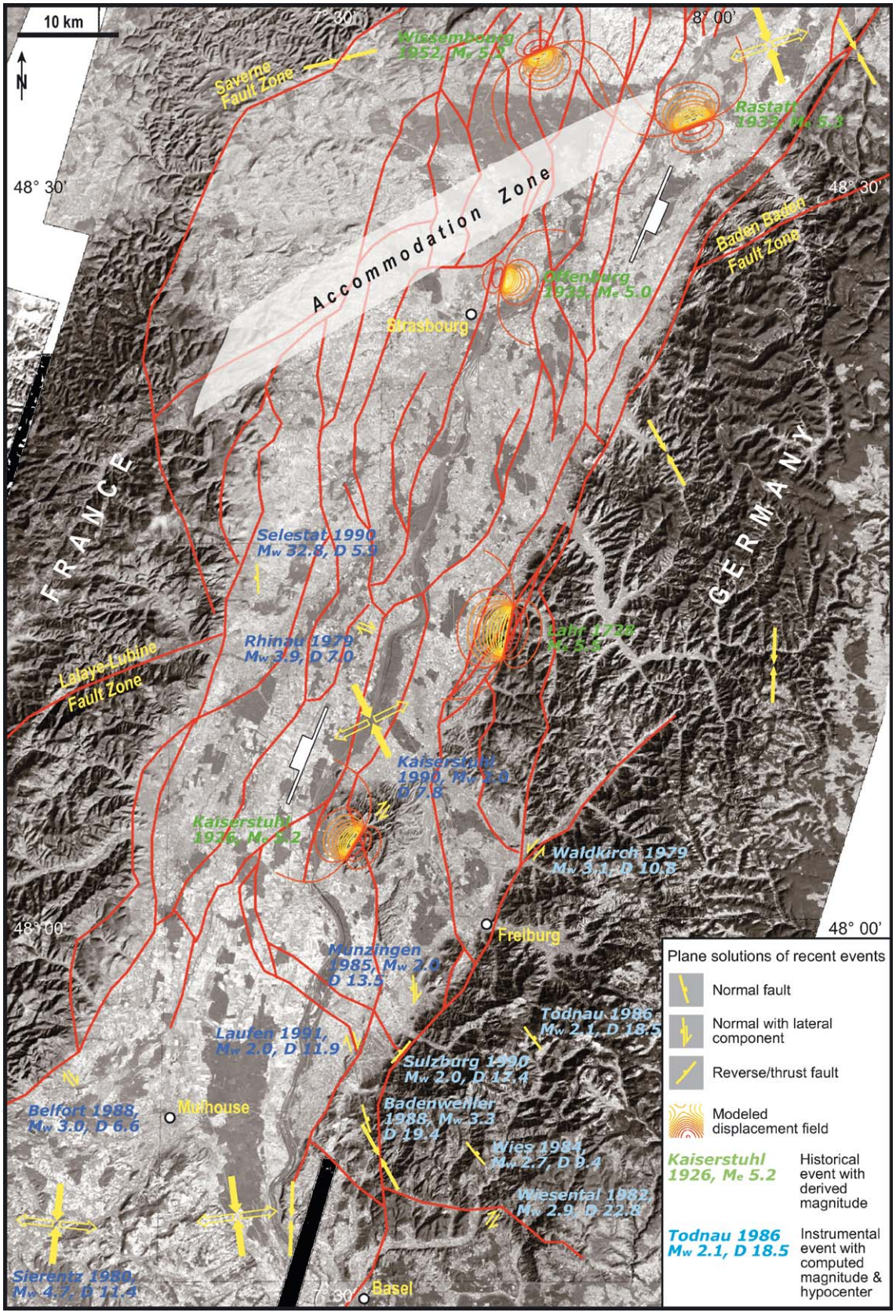
10 km
N
7° 30'
8° 00'
48° 30'
48° 00'
Wissembourg 1952, Me 5.5
Saverne Fault Zone
Rastatt 1933, Me 5.3
Accommodation Zone
Baden Baden Fault Zone
Offenburg 1945, Me 5.0
Strasbourg
FRANCE
GERMANY
Selestat 1990 Mw 32.8, D 5.3
Rhinau 1979 Mw 3.9, D 7.0
Lahr 1724 Me 5.5
Lalaye-Lubine Fault Zone
Kaiserstuhl 1990, Mw 3.0 D 7.8
Kaiserstuhl 1926, Me 5.2
Waldkirch 1979 Mw 3.1, D 10.8
Freiburg
Münzingen 1985, Mw 2.0 D 13.5
Todnau 1986 Mw 2.1, D 18.5
Laufen 1991, Mw 2.0, D 11.9
Sulzburg 1990 Mw 2.0, D 12.4
Belfort 1988, Mw 3.0, D 6.6
Mulhouse
Badenweiler 1988, Mw 3.3 D 19.4
Wies 1984, Mw 2.7, D 9.4
Wiesental 1982 Mw 2.9, D 22.8
Sierentz 1980, Mw 4.7, D 11.4
Basel
Plane solutions of recent events
Normal fault
Normal with lateral component
Reverse/thrust fault
Modeled displacement field
Kaiserstuhl 1926, Me 5.2
Historical event with derived magnitude
Todnau 1986 Mw 2.1, D 18.5
Instrumental event with computed magnitude & hypocenter

promising in terms of the seismotectonic objectives of this work.

4. Geological role of three case-studies

4.1. Macroseismic field of the 28/06/1926 Kaiserstuhl event

Located close to the extinct volcanic complex (Menillet, 1995) NW of Freiburg, this earthquake yielded a significant I_E of VII. Neither foreshocks or aftershocks were seemingly recorded. This event proved to be a viable template for our purposes in the S Upper Rhine Graben, due to the amount of available felt reports, their dense distribution across the basin and the reliability offered by the relatively recent year of documentation. Fig. 8 explains the features of the computed solution and its scenario.

This event yielded 545 intensity points, excluding the 0.0 values (184, i.e. 25.09% of the listed localities). The latter recorded values are either of unknown damage or absence of it and their majority lies within the French border. Although felt reports cover a very wide area if we consider the relatively moderate 5.2 M_e, we notice that the VI/VII region, somewhat extending along NW–SE, is very close to the epicenter (<15 km), if compared to the whole area. This suggests a sharp intensity decay along the trend of the Rhine Graben. The macroseismic pattern tends to favor the graben foothills, in as much as this is the most populated area and thus these piedmont areas exert some predominance on the overall recorded intensities.

In order to identify a possible fault trace, we employed FaultMapper 3.2, an in-house code developed by Dr. Roberto Basili at INGV (Istituto Nazionale di Geofisica e Vulcanologia). Since no surface rupture was found in the field neither was it described in the literature, we temptatively input a top depth of the fault plane within the first upper km (−0.5) from the ground to obtain a 4.2 bottom depth, where a prospective hypocenter could be located.

One point can be raised as per the sensitivity of Boxer© in weighting the input data. To isolate the epicenter, the code screens the dataset to locate at least four points with equal maximum intensity. For this event, only two points yield a I_{MSK} = VII, so the search window was automatically enlarged to the next lower intensity class (in this case, VI). Among these localities, we realized that Bru (in red in Fig. 8) returned a value of VI within a cluster of IV adjoining intensity points. Bru is ~50 km W of the epicenter, falling within the IV isoseismal sector, while most V values can be found on the Vosgian border fault. Other intensity points found in valleys nearby the basin show much smaller I_{MSK} (III–IV) despite their proximity to the Kaiserstuhl.

When taking Bru into account, the solution computed by Boxer yielded a 5.17 M_e and a N57.1° box azimuth. Surprisingly, the box rotates to N30.3° without the value associated to Bru. The geometrical and intensity relationships between this locality and the prospective epicenter/box were such that a single datapoint, although quite distant from the Kaiserstuhl, could remarkably influence the expected projection of the computed source. The scatter nature of data around Bru itself contributed to associate to the latter a tangible distance weight. However, since (a) this locality is quite far from the macroseismic centroid and (b) it sits in an inner valley on the W flank of the Vosges Mountains, we believe that the value had likely been overestimated due to site effects (Giner et al., 2002; Lee and Kim, 2002). Therefore, we preferred to drop it from our final computation, although we chose to display the two solutions to show the sensitivity of the procedure.

4.2. Kaiserstuhl 1926 and Rastatt 1933: comparison of possible site effects

Another event that yielded an interesting M_e (5.3) and was based on a wide macroseismic field (446 intensity points) is represented by the case of Rastatt 08/02/1933. Ahorner (1975) indicates a $M = 5.4$ event with left-lateral solution and a prospective focal depth at 4 km (6 km in Ahorner et al., 1970). Thus, for our seismogenic source we opted to consider a base of fault plane (and potential hypocenter) compatible with the aspect ratio for such magnitude and within the range suggested by the above Authors.

Fig. 9 compares the isoseismal pattern of this earthquake (white dashed contours) when associated to the one belonging to the Kaiserstuhl 28/06/1926 (red dashed isolines) one. They were compared due to their compatible intensity scenario, similar parameters of the computed source and respective distance so as to evaluate the common damage pattern across the graben.

Distribution of felt reports for both events was interpolated (using Carlson and Foley's 1991 algorithm) to observe the overlap of the shared damage area and

Fig. 7. Fault pattern of the overall research area, partly arising from the database assembled by Behrmann et al. (2003 and references therein). Most faults stem out of the extensive borehole dataset built up by these authors, who also validated these structures via 3D kinematic restoration. The largest (I_{MSK} > 6.0) historical seismic events are plotted with their displacement field (following the algorithm by Okada 1985 and 1992). Also on this map, we plotted relevant instrumental events (after Bonjer, 1997; Plenefisch and Bonjer, 1997: see Table 2), together with computed fault plane solutions and present-day stress orientations (from Schumacher, 2002 and references therein). Large white dip marks indicate vergence of basement N and S of the oblique rift accommodation zone (as per Behrmann et al., 2003) (*SPOT data courtesy of CNES/SPOT Image© 1992–1994*).

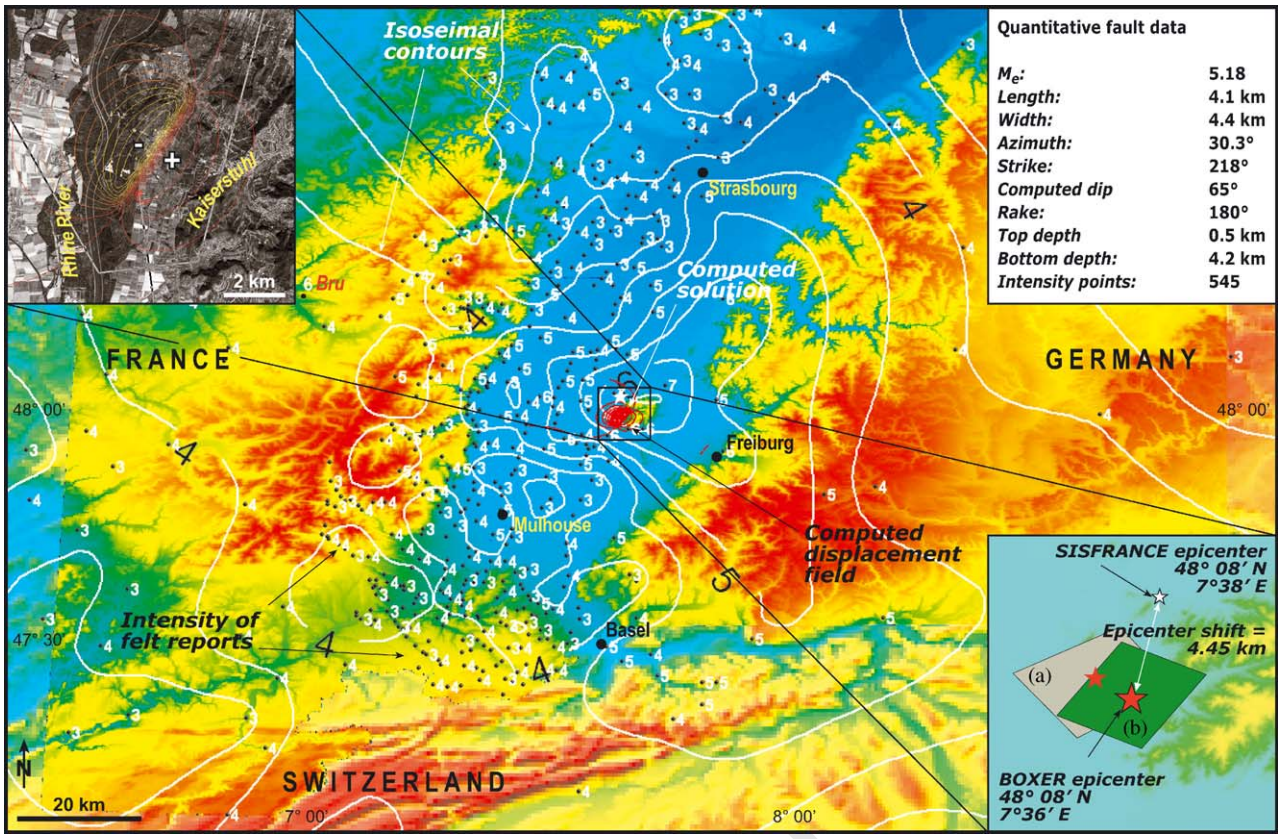

Fig. 8. Felt reports and interpolated isoseismal pattern caused by the 1926 Kaiserstuhl event ($M_e = 5.2$). Inset in upper left indicates imprint of the potential solution computed by Boxer© and its displacement field modeled as per Okada (1985 and 1992) procedure. Inset in lower right shows the sensitivity of Boxer© to unexpected felt reports and potential localized site effects. The Kaiserstuhl event entailed a VI I_{MSK} value in the locality of Bru (in red), on the Vosges Mountains. Here we show the solution for the seismogenic source either (a) taking or (b) not into consideration this isolated value. Eventually, we adopted the solution without Bru, on the realistic assumption that the VI intensity was overestimated (*SPOT data courtesy of CNES/SPOT Image© 1992–1994*).

also to ascertain any relationships with the basin arrangement. To achieve this, we incorporated the thickness of the Quaternary deposits, as probed by a borehole campaign by Bartz (1974). The red profile in Fig. 9 shows the maximum depths of the Quaternary base. Such features therefore represent three depocenters: between Mulhouse and the Kaiserstuhl volcano; around Strasbourg and the major one (partly out of map), W of Heidelberg and N of the Lalaye–Lubine–Baden Baden Fault Zone.

The distribution of felt reports for these earthquakes highlights the possible consistency between the funnel-shaped sub-basin (towards the SW border fault of the Upper Rhine Graben) and the overall arrangement of the reconstructed isoseismals. Such superposition is conceivably due to the vastly inhabited basin, thus causing a geographical predominance of lowland areas in terms of available felt reports. The graben hosts a relatively sedimentary cover (320 m max. for the Quaternary; Bartz, 1974), likely to enhance the damage factor (see Field, 1996; Horike et al., 2001), thus influencing the position of the prospective seismogenic source computed by Boxer. Three cross-sections highlight the sensible difference between the felt reports distribution. The upper one runs across the graben, from Mulhouse to Heidelberg and shows the peaks due to the epicentral intensities. Both events show a remarkable cyclicity in the intensity decay (as defined by Esposito et al., 1992), possibly in connection with the two depocenters. Depocenter 1 likely controlled the sharp I_{MSK} decrease towards S for the Kaiserstuhl earthquake, while depocenter 2 can be associated to the sustained intensity values for the Rastatt event.

The parallel profiles we show for the outer flanks of the graben indicate a much smoother isoseismal distribution. E of the basin, the Kaiserstuhl event displays a peak in the vicinity of its epicenter and a gentle decay N-wards; a similar pattern can be observed for the Rastatt event. On the W shoulder, the intensity distribution of the Kaiserstuhl earthquake is essentially smooth, while the Rastatt intensities show a variable pattern. A peak is visible in correspondence of the large Wasselonne–Saverne lowlands, probably indicating a control exerted by the alluvial infill. No direct link with

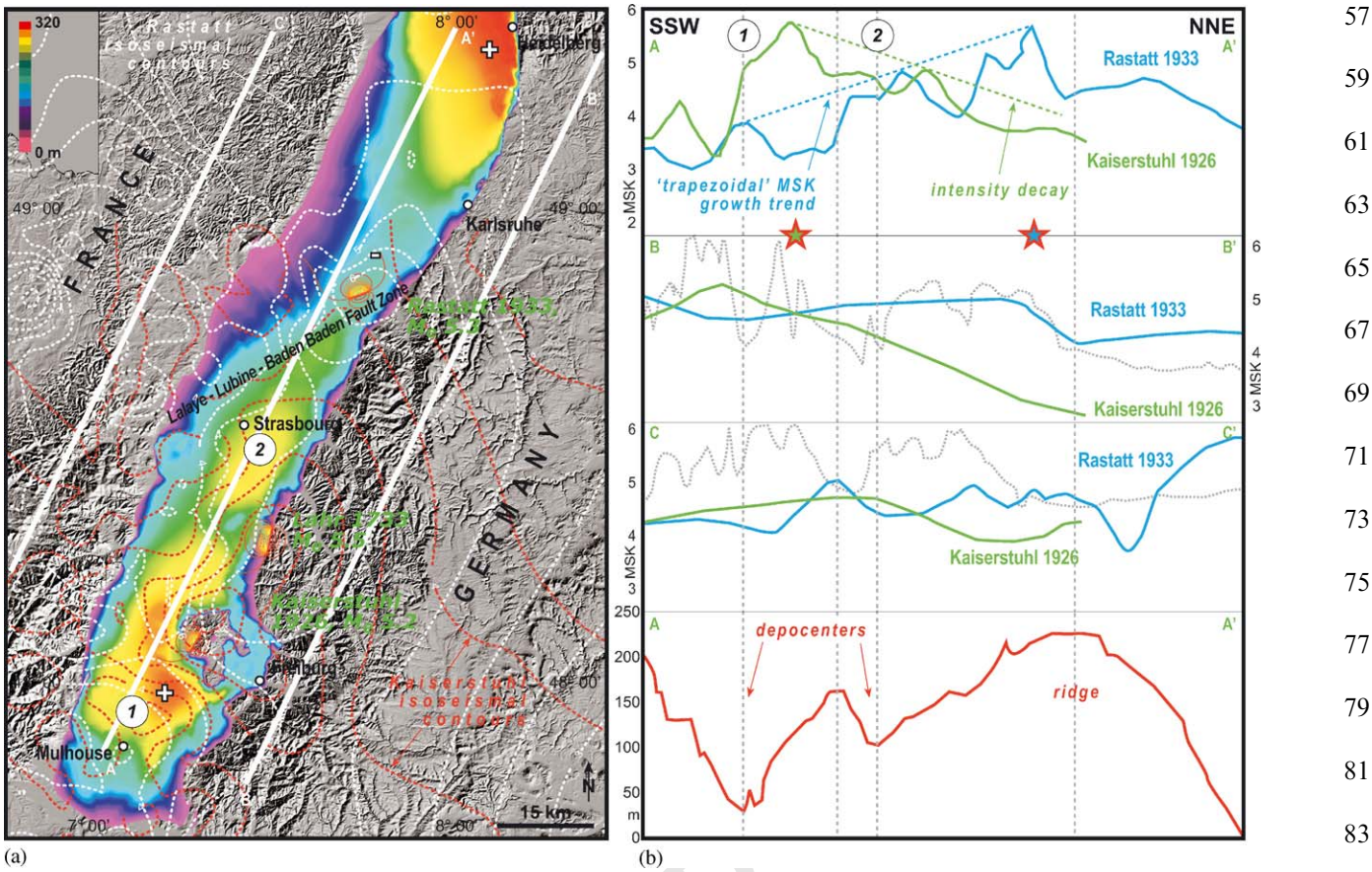

Fig. 9. (a) Relationship between the thickness of Quaternary deposits (digitized and georeferenced: data from Bartz, 1974) and the overall isoseismal pattern of two significant historical events (Kaiserstuhl 1926, $M_e = 5.2$ & Rastatt 1933, $M_e = 5.3$, red and white dashed lines respectively). Color bar in the upper left indicates depth of Quaternary base. (b) SSW-NNE profiles, intercepting the distribution of felt reports for the above earthquakes. The upper one shows a peculiar (and somewhat symmetrical) peak pattern on the two isoseismal fields. For the Kaiserstuhl 1926 event, such feature is likely to be caused by the spatially variable thickness of the Quaternary terrains (depocenters 1 and 2). Conversely, on the rift shoulders, the felt reports distribution is much smoother, even within short range from either epicenter. Topographic profiles E and W of the graben are shown in dotted grey line.

topography (dashed grey line) is observable in the overall area.

In sum, despite the sound statistical philosophy Boxer© delivers to ascertain a prospective source, the nature and the inner reliability of historical felt reports are neither univocal nor absolute. As known, local amplifications and overall site effects (Borcherdt, 2002) may affect the macroseismic pattern. Such limit should clearly be taken into account (see previous paragraph) when approaching the geometrical arrangement of felt reports to seek quantitative information about a prospective seismogenic source.

4.3. Seismotectonic scenario of the Lahr 1728 event

This earthquake, located on the E border fault ca. 30 km N of Freiburg and documented on 03/08/1728, is the largest one in the SISFRANCE catalog. Out of 76 available felt reports, only 30 proved to be valid ones (16 in Germany), while the rest were either reported as 0 or bearing undefined damage. Leydecker (1986 and 2003) specifies an inferred focal depth of 16 km. Since we are unsure about the reliability of such value given the age of this earthquake, we believe that a depth of 10 km, if conservative, is compatible with the damage scenario and the constraints of the E border fault of the graben.

Boxer computed a M_e of 5.5, the highest magnitude if compared with the rest of historical and instrumental events across the whole study area. Such magnitude is also consistent with the lower threshold estimated by Valensise and Pantosti (2001a, b) for viable seismogenic sources. While we cannot document that this single event caused either ground-warping or surface rupture (not directly evident on the field), the activity of such segment of the border fault along the SE margin of the graben clearly entailed cumulative deformation through recent geologic time.

Fig. 10a locates the computed displacement field for the solution provided by Boxer© with respect to the coalescing border fault system, its topographic signature

and the pre-Quaternary isopachs. Colored overlay represents the thickness of the Quaternary deposits. A saddle (light blue), separating two depocenters (yellow), faces the prospective fault. Such feature is also visible on a cross-section (Fig. 10e) showing the presence of pre-Quaternary alluvial aprons. The potential source computed by Boxer© is remarkably parallel to the fault system flanking the graben. Fig. 10b and c highlight the physiography of the border between present-day topography of the graben margin and the underlying bottom of the alluvial body. In these oblique views, the parallel strands of the border fault are partly concealed by the dissected landscape. In the lowlands that can be seen in the base of the Quaternary, we recognized a scarp a few km W of the prospective source, likely due to Early Quaternary paleo-drainage. Fig. 10d corresponds to a view from WSW, showing that the maximum displacement for such a computed box occurs nearby a depression (light blue), in part also visible from the orthogonal view of Fig. 10c. The overall displacement field develops across the margin topography altered by the border fault system.

According to these results, the prospective seismogenic source could have acted as a connecting splay between the multiple breached relay that constitute the SE border fault. From a macroseismic viewpoint, however, we can envisage that the source is not entirely corresponding to the strands of the border system due to either: (a) a certain degree of uncertainties in the location and I_{MSK} of the felt reports (as was the case for the Kaiserstuhl 1926 event), or: (b) the scale of our investigation is finer than the geographical resolution offered by the macroseismic data set.

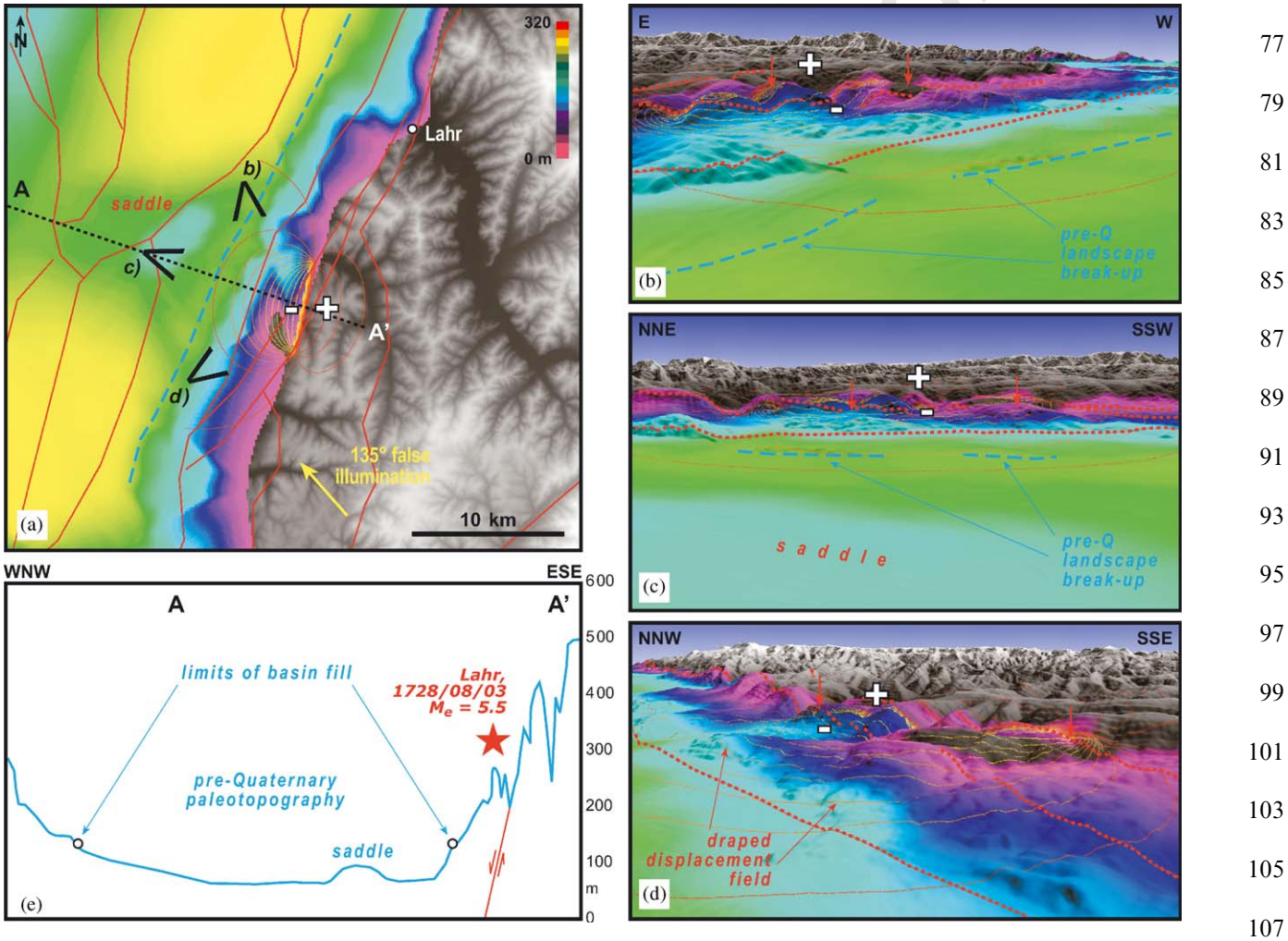

Fig. 10. Relationship between pre-Quaternary paleotopography (after Bartz, 1974), known fault pattern (after Behrmann et al., 2003) and computed displacement field for the prospective seismogenic source of the Lahr 1728 event ($M_e = 5.5$, the largest in the region). Colored overlay represents thickness of the Quaternary cover (see Fig. 9). (a) locates the Boxer© solution upon the border fault; (b), (c) and (d) show 3D fly throughs above inferred fault with respect to pre-Quaternary paleo-landscape and projected trace of subsurface fracture mesh (thick red dotted lines); (e) shows a 2D profile across the pre-Quaternary paleosurface. Notice the blue saddle facing the prospective fault. Vertical red arrows show trace of the solution indicated by Boxer©. DEM vertical exaggeration: 200%.

5. Potential seismogenic sources in southern Upper Rhine Graben

Boxer© was devised essentially for the tectonic scenario of Southern Europe and applications were particularly successful for the Italian peninsula (Valensise and Pantosti, 2001b). However, the procedure takes into account several physical constraints pertaining to the macroseismic record and to the statistical pitfalls. These allow a fair degree of control also for earthquakes with felt report patterns that can be expected in a low seismicity region as the S Upper Rhine Graben. The available dataset allowed to analyze 5 prospective sources that proved to yield a realistic overprint onto the structural setup of the Upper Rhine Graben, both at the splay and at the border fault scale.

While the magnitudes obtained may not allow a tangible ground-warping potential to these earthquakes or, if any, it was concealed by exogenous factors, the cumulative deformation through time that we can associate to the studied events is substantiated by their suitability with the fracture pattern of the graben and their compatibility with background seismicity. Furthermore, this first attempt to define potential seismogenic sources throughout historical seismic record in the Rhinegraben highlighted the contrast between the present-day geomorphic scenario on the W border (seismically silent, within the limits of current knowledge) and the overall minor to moderate seismicity in the E sector of the graben. The latter is presented in the literature as not being the border fault system responsible for the geometry of the southern half-graben.

From past experiences in Europe about continental seismicity in regions thought to be of low seismic activity (Bonjer et al., 1984; Loew et al., 1989; Meyer et al., 1994; Bonjer, 1997), we learnt that low seismicity does not imply low seismic risk (Camelbeeck and Meghraoui, 1996). Therefore, realistic assessment of likely seismogenic sources for constrained earthquakes can provide a template to recognize faults that can prospectively trigger a seismic event in areas where ongoing deformation occurs yet no relevant seismic history was recorded. Our research demonstrated that viable and mathematically consistent fault solutions devise a prospective scenario differing from the subtle landscape indicators. Also, these results underline that the procedure followed is capable of appropriately filtering uncertain locations and, possibly, a specific bias caused by site effects. Therefore, a potential seismogenic source gains a geologically realistic status, even in a region with thick sediment cover and low and scattered seismic record.

We believe that, while limits to the resolution of viable seismogenic structures are intrinsic to the geodynamic scenario of this region and the completeness of the available macroseismic pattern, the solutions we isolated show that this procedure can be positively applied to the southern Upper Rhine Graben. To this end, a backward extension of the historical catalogue is likely to supply key insight into the broader framework of the known structures and their seismogenic potential.

Acknowledgement

This work originated from a post-doctoral research stay of UF at BRGM (Bureau de Recherches Geologiques et Minieres, Orleans, France) in 2002. Support and clever guidance from his supervisors (herewith co-Authors) and from Dr. Sebastien Carretier and Dr. Christine King were very appreciated. The contract funding UF was part of the ENTEC (Environmental Tectonics) Research & Training Network, within the EU V° Framework Programme. UF wishes to graciously acknowledge Prof. Sierd Cloetingh (Vrije Universiteit Amsterdam), head of the Network, for his appreciative outreach. Likewise, UF wishes to thank his colleagues of the ENTEC Network, particularly Dr. Ralph Hinsch (Universität Wien), Dr. Guillaume Bertrand (now at BRGM), Mr. Gideon Lopes Cardozo (I.P.G. Strasbourg) and Mr. Kamil Ustaszewski (Universität Basel) for their human aptitude and *vicinitas*. Dr. Emmanuel Baroux (INGV) was instrumental concerning the Boxer© features; Dr. Salvatore Barba and Dr. Roberto Basili (same institution) respectively helped with critical interpretation of *b*-values and provided with helpful insight into the final version of the manuscript. Finally, we acknowledge the very constructive review by Dr. Kurt Decker (Universität Wien).

Appendix A. Boxer© philosophy and structure

Here we summarize some basic points explained by Gasperini et al. (1999) concerning the concept behind Boxer©. These Authors underline the difference between the instrumental epicenter (determined by triangulation among recording stations) and the macroseismic one, for which a comprehensive definition is still debated. For damaging earthquakes ($M > 5.5$), such epicenter could be individuated as the barycenter of the region yielding the largest earthquake effects. Boxer© copes with the task of epicenter location and parameters computation to smooth away local site amplification, biased assigned intensity etc., employing a central tendency estimator (Gasperini et al., 1999). Input values are first subdivided into intensity classes; a first downsizing is operated by approximating all intermediate values (eg., 6.5 or VI–VII) to the lower threshold. Then, localities reporting the highest observed intensity (I_{max}) are separated for subsequent calculations. When I_{max} falls within full values (eg., VII–VIII), the searching

radius is increased to include also localities that reported full values immediately lower than I_{max}. Should this number of sites be insufficient for source computation, the code will also seek lower records up to $I_{max}-1$. Finally, the epicentral coordinates are chosen among the first 75% of the available localities.

Some sort of uncertainty also remains with the Boxer© algorithm itself. To this end, the sum of square residuals between the coordinates of the chosen felt reports and those of the inferred epicenter are computed too. Such parameter, although not directly employed in the source calculation, is a viable internal tool to control the reliability of the estimate.

Since there is no yet accepted physical relationship between magnitude and intensity data (Gasperini et al., 1999), a statistical approach is required to compute M_e, as the one devised by Gasperini et al. (1999). The macroseismic epicenter, already computed in the first place, yields an intensity I_0 assumed to be equal to I_{max} if at least two data with that intensity are found; otherwise, I_0 is set to the second highest observed value, with a lower threshold at $I_{max}-1$. Then, the distance between the epicenter and each available locality is computed; this information will be employed to derive the average R_I for each value, using the median as central tendency estimator. A bivariated weighted regression is fitted over the events for each intensity level (Gasperini et al., 1999):

$$M = a + bI_0^2 + c\log^2(A_I), \quad (1)$$

where A_I is the area of a circle of radius R_I. The weight assigned to each observation considers the uncertainty of M, the level of knowledge of the given event and the amount of observations used to average the distances.

Stirling et al. (2002) show that the Wells and Coppersmith (1994) algorithm, employed by Boxer© to infer M_e from historical felt reports, tends to underestimate magnitude when information for the same earthquake is cross-checked with direct geological evidence (paleoseismological data). Therefore, to summarize the above points, Boxer© results may possibly yield a conservative approach to determine source magnitude, something facilitated by the rigorous down-trimming exerted onto input data. However, the most relevant tool to shape Boxer results is to alter the input parameters, specifically the distance weight and the radius method to compute M_e. The former determines the azimuth of the prospective source, following the algorithm (Gasperini et al., 1999):

$$\Delta I = a + b\sqrt[3]{D}, \quad (2)$$

where ΔI is the difference between epicentral and local intensity and D is the epicentral distance. The latter entails magnitude calculation following the algorithm (1) previously explained, using 3 weight parameters for each class of intensity.

Appendix B. Interpolation of sparse macroseismic data

Felt reports individuate locations for which a certain damage was described. In order to compute the isoseismal pattern, we interpolated such dataset, following the formulae devised by Carlson and Foley (1991) and as recently employed in Fracassi (2001). The topographic surface onto which our felt reports lie is approximated by a plane containing a number n of distinct points, so that these can be expressed as (x_i,y_i), with $i = 1, 2, \ldots n$. These are defined *scattered data points* and a function capable of associating them is a *scattered data interpolation* (Carlson and Foley, 1991). Generally, these data are assumed to be randomly distributed on a plane, i.e. they do not form a regular grid. The above authors in fact concentrated onto points that tend to sit along paths in a given plane, thus introducing the concept of *track data*. Such tracks need not be straight lines; the basic requirement is that two adjoining points along the same track are of some orders of magnitude closer than two points belonging to two distinct tracks (Carlson and Foley, 1991).

To effectively interpolate such scattered data, these authors presented the radial basis function, described as follows:

$$F(x,y) = \sum_{i=1}^{n} \lambda_i \Phi[||(x,y) - (x_i,y_i)||], \quad (3)$$

where Φ is the chosen interpolator and λ_i is a data set coefficient. For macroseismic felt reports, we opted for the Multiquadratic method, recommended as the most suited to produce a geologically wise surface:

$$\Phi[||(x,y) - (x_i,y_i)||] = \sqrt{||(x,y) - (x_i,y_i)||^2 + R^2}, \quad (4)$$

where the first member of the polynomial under square root is the anysotropic relative distance from a datapoint to the node of the interpolated grid and R^2 is a smoothing factor. The above is an exact interpolation procedure, so it attempts to honor the original sparse data values (Carlson and Foley, 1991).

Appendix C. Modeling the displacement field

Dip-slip faulting is a structural process that generates relief, a fact commonly accepted in its basic principles (Savage and Hastie, 1966; King et al., 1988a, b). An upper layer containing an earthquake fault (or a prospective seismogenic source, for our purposes) retains strength indefinitely and acts elastically but the material beneath relaxes stress at a rate determined by its viscosity (King et al., 1988a). Consequently, deformation sums through geological time and changes between seismic events on the same source. Originally horizontal layers can be considered as fossilized leveling

lines that record sufficiently large cumulative displacement. On the ground of these considerations, it is possible to compute models as close as possible to the studied structures. These develop within the physical constraints posed by long-term effective elastic thickness (T_E) of the crust, while the asymmetry of uplift to subsidence is notably controlled by sediment budget within a newly formed basin (King et al., 1988a).

The modeling approach was based on the formulations developed by Okada (1985, 1992), in which fault patches are assumed to be planar, with uniform slip, embedded in a uniform elastic half-space. Displacement field $u_i(x_1, x_2, x_3)$, due to a dislocation $\Delta u_j(\xi_1, \xi_2, \xi_3)$ across a surface Σ in an isotropic medium is given by (Okada, 1992):

$$u_i = \frac{1}{F} \int \int_{\Sigma} \Delta u_j \left[\lambda \delta_{jk} \frac{\partial u_i^n}{\partial \xi_n} + \mu \left(\frac{\partial u_i^j}{\partial \xi_k} + \frac{\partial u_i^k}{\partial \xi_j} \right) \right] v_k \, d\Sigma, \quad (5)$$

where v_k is the direction cosine of the normal to the surface element $d\Sigma$. Therefore, internal displacement field u° for dip-slip faulting is expressed as follows:

$$u^\circ = \frac{M_0}{F} \left[\left(\frac{\partial u^2}{\partial \xi_3} + \frac{\partial u^3}{\partial \xi_2} \right) \cos 2\delta + \left(\frac{\partial u^3}{\partial \xi_3} - \frac{\partial u^2}{\partial \xi_2} \right) \sin 2\delta \right]. \quad (6)$$

Elastic parameters (Lame's constants λ and μ) were both kept equal to 1. The amount of slip was kept constant and equal to 0.3 m in all models. Strike, dip, rake, length, width, depth, average slip of the suspected causative faults are derived from input of fault tips coordinates into FaultMapper 3.2. Aspect ratio (Length/Width) to define the fault plane is derived from empirical relationships of coseismic rupture dimensions from Wells and Coppersmith (1994). Relationships between fault area, earthquake magnitude and seismic moment are those by Kanamori and Anderson (1975). Empirical constant factors employed to derive M_w from the inferred seismogenic source whose fault kinematics and plane area is known (or suspected) is (Wells and Coppersmith, 1994):

$$M_w = a + b \log A \quad (7)$$

following the parameters as per Table 4. The overall mathematical procedure is incorporated into GPS Scenario©, an in-house command-line code developed by Dr. Roberto Basili (INGV).

Table 4
Parameters to compute M_w from a prospective seismogenic source on the ground of known fault area (from: Wells and Coppersmith, 1994)

	Normal	Reverse	Strike-slip	All
a	3.93	4.33	3.98	4.07
b	1.02	0.90	1.02	0.98
A	Fault plane area (km^2) = Length (L) × Width (W)			

References

Ahorner, L., 1975. Present-day stress field and seismotectonic block movements along major fault zones in Central Europe. Tectonophysics 29 (1), 233–249.

Ahorner, L., Murawski, H., Schneider, G., 1970. Die Verbreitung von schadenverursachenden Erdbeben auf dem Gebiet der Bundesrepublik Deutschland. Versuch einer seismologischen Regionalisierung (The distribution of earthquakes causing damage on the territory of the Federal Republic of Germany. An attempt of seismic regionalisation). Zeitschrift für Geophysik 36, 313–346.

Albarello, D., Camassi, R., Rebez, A., 2001. Detection of Space and Time Heterogeneity in the Completeness of a Seismic Catalog by a Statistical Approach: An Application to the Italian Area. Bulletin of the Seismological Society of America 91 (6), 1694–1703.

Bano, M., Marquis, G., Nivière, B., Maurin, J.-C., Cushing, M., 2000. Investigating alluvial and tectonic features with ground penetrating radar and analysing diffractions patterns. Journal of Applied Geophysics 43 (1), 33–42.

Bartz, J., 1974. Die Mächtigkeit des Quartärs im Oberrheingraben. In: Illies, J.H., Fuchs, K. (Eds.), Approaches to Taphrogenesis. Schweitzerbarth Verlagen, pp. 78–87.

Becker, A., 2000. The Jura Mountains—an active foreland fold-and-thrust belt? Tectonophysics 321, 381–406.

Behrmann, J.H., Hermann, O., Horstmann, M., Tanner, D.C., Bertrand, G., 2003. Anatomy and kinematics of oblique continental rifting revealed: a 3D case study of the SE Upper Rhine Graben (Germany). American Association of Petroleum Geologists Bulletin 87 (7), 1105–1121.

Blake, A., 1941. On the estimation of focal depth from macroseismic data. Bulletin of the Seismological Society of America 31, 225–231.

Bois, C., 1993. Initiation and evolution of the Oligo-Miocene rift basins of southwestern Europe: contribution of deep seismic reflection profiling. Tectonophysics 226, 227–252.

Bonjer, K.-P., 1997. Seismicity pattern and style of seismic faulting at the eastern borderfault of the southern Rhine Graben. Tectonophysics 275 (1), 41–69.

Bonjer, K.-P., Gelbke, C., Gilg, B., Rouland, D., Mayer-Rosa, D., Massinon, B., 1984. Seismicity and dynamics of the Upper Rhinegraben. Journal of Geophysics 55 (1), 1–12.

Borcherdt, R.D., 2002. Empirical evidence for acceleration-dependent amplification factors. Bulletin of the Seismological Society of America 92 (2), 761–782.

Boschi, E., Guidoboni, E., Ferrari, G., Mariotti, D., Valensise, G., Gasperini, P., (Eds.), 2000, Catalogue of strong Italian earthquakes. Annali di Geofisica 43, 4.

Brace, W.F., Byerlee, J.D., 1966. Stick-slip as a mechanism for earthquakes. Science 153, 990–992.

Briquet, A., 1931. Le Quaternaire de l'Alsace. Bulletin de la Société Géologique de France 4 (XXX-62), 977–1014.

Brun, J.P., Gutscher, M.-A., DEKORP-ECORS Team, 1992. Deep crustal structure of the Rhine Graben from DEKORP–ECORS seismic reflection data: a summary. Tectonophysics 208, 139–147.

Brüstle, A., 2002. Morphotectonic analysis of the Freiburg i. Br. region in the Upper Rhine Graben, unpublished Diplomarbeit Thesis, Bureau de Recherches Geologiques et Minieres and Universität zu Köln, 83p.

Camelbeeck, T., Meghraoui, M., 1996. Large earthquakes in northern Europe more likely than once thought. Eos 77 (42), 405–409.

Carena, S., Suppe, J., Kao, H., 2002. Active detachment of Taiwan illuminated by small earthquakes and its control of first-order topography. Geology 30 (10), 935–938.

Carlson, R.E., Foley, T.A., 1991. Radial basis interpolation methods on track data. Lawrence Livermore National Laboratory, UCRL-JC-1074238.

Chorowicz, J., Deffontaines, B., 1993. Transfer faults and pull-apart model in the rhinegraben from analysis of multisource data. Journal of Geophysical Research 98 (B8), 14.339–14.351.

Clauser, C., Griesshaber, E., Neugebauer, H.J., 2002. Decoupled thermal and mantle helium anomalies: Implications for the transport regime in continental rift zones. Journal of Geophysical Research 107 (B11), 2269 doi: 10.1029/2001JB000675.

Derer, C.E., 2003. Tectono-sedimentary evolution of the northern Upper Rhine Graben (Germany), with special regard to the early syn-rift stage. Rheinischen Friedrich-Wilhelms-Universitt Bonn, 99p.

Esposito, E., Luongo, G., Marturano, A., Porfido, S., 1988. I terremoti recenti dal 1980 al 1986 nell'Appennino Meridionale. Memorie della Società Geologica Italiana 41, 1117–1128.

Esposito, E., Porfido, S., Luongo, G., Petrazzoli, S.M., 1992. Damage scenario induced by the major seismic events from the XV to XIX century in Naples city with particular reference to the seismic response, Proceedings of the "10th World Conference on Earthquake Engineering", A.A. Balkema Publishing House, Rotterdam, pp. 1075–1080.

Esposito, E., Laurelli, L., Porfido, S., 1995. Damage pattern in historical centres: Isernia, an Example in Southern Italy. Annali di Geofisica 38 (5–6), 663–677.

Field, E.H., 1996. Spectral amplification in a sediment-filled valley exhibiting clear basin-edge induced waves. Bulletin of the Seismological Society of America 86 (4), 991–1005.

Fracassi, U., 2001. Morphotectonic signature of the Campo Imperatore intermontane basin (Central Apennines): implications for the seismotectonics of Central Italy, unpublished Ph.D. Thesis, Università di Firenze.

Gasperini, P., Ferrari, G., 2000. Deriving numerical estimates from descriptive information: the computation of earthquake parameters. In: Boschi, E., Guidoboni, E., Ferrari, G., Mariotti, D., Valensise, G., Gasperini, P. (Eds.), Catalogue of strong italian earthquakes from 461 B.C. to 1997. Annali di Geofisica 43(4), 729–746.

Gasperini, P., Valensise, G., 2000. From earthquake intensities to earthquake sources: extending the contribution of historical seismology to seismotectonic studies. In: Boschi, E., Guidoboni, E., Ferrari, G., Mariotti, D., Valensise, G., Gasperini, P. (Eds.), Catalogue of strong Italian earthquakes from 461 B.C. to 1997. Annali di Geofisica 43(4), 765–785.

Gasperini, P., Bernardini, F., Valensise, G., Boschi, E., 1999. Defining Seismogenic Sources from Historical Earthquake Felt Reports. Bulletin of the Seismological Society of America 89 (1), 94–110.

Giner, J.J., Molina, S., Jauregui, P., 2002. Advantages of using sensitivity analysis in seismic hazard assessment: a case study of sites in Southern and Eastern Spain. Bulletin of the Seismological Society of America 92 (2), 543–554.

Grünthal, G. (Ed.), 1998. European Macroseismic Scale 1998: EMS-98, 2nd ed., Cahiers du Centre Europèen de Géodynamique et de Séismologie, 15.

Gruppo di Lavoro CPTI, 1999. Catalogo Parametrico dei Terremoti Italiani, ING – GNDT – SGA – SSN, Bologna.

Hetzel, R., Niedermann, S., Tap, M., Kublik, P.W., Ivy-Ochs, S., Gao, B., Strecker, M.R., 2002. Low slip rates and long-term preservation of geomorphic features in Central Asia. Nature 417, 428–432.

Horike, M., Zhao, B., Kawase, H., 2001. Comparison of Site Response Characteristics Inferred from Microtremors and Earthquake Shear Waves. Bulletin of the Seismological Society of America 91 (6), 1526–1536.

Illies, J.H., Greiner, G., 1978. Rhinegraben and the Alpine system. Geological Society of America Bulletin 89, 770–782.

Kanamori, H., Anderson, D.L., 1975. Theoretical basis of some empirical relations in seismology. Bulletin of the Seismological Society of America 65, 1073–1095.

Keller, E.A., Pinter, N., 2002. Active Tectonics—Earthquake, Uplift and Landscape, 2nd ed., Prentice-Hall, Englewood Cliffs, NJ, 362pp.

King, G.P., Stein, R.S., Rundle, J.B., 1988a. The growth of geological structures by repeated earthquakes—1. Conceptual framework. Journal of Geophysical Research 93 (B11), 13.307–13.318.

King, G.P., Stein, R.S., Rundle, J.B., 1988b. The growth of geological structures by repeated earthquakes—2. Field examples of continental dip-slip faults. Journal of Geophysical Research 93 (B11), 13.319–13.331.

Kovesligethy, R., 1907. Seismicher Starkegrad und Intensitat der Beben. Gerlands Beitr. z. Geophysik 8, 363–366.

Lambert, J., Winter, T., this volume, Revisiting the 1356 Basel Earthquake: uncertainties on the area of maximum damages.

Lambert, J., Levret-Albaret, A., Cushing, M., Durouchoux, C., 1996. Mille ans de séismes en France. Ouest Editions, 78pp.

Lee, K., Kim, J.-K., 2002. Intensity Attenuation in the Sino-Korean Craton. Bulletin of the Seismological Society of America 92 (2), 783–793.

Leeder, M.R., Gawthorpe, R.L., 1987. Sedimentary models for extensional tilt-block/half-graben basins. In: Coward, M.P., Dewey, J.F., Hancock P.L. (Eds.), Continental Extensional Tectonics. Geological Society of London Special Publications, 28, 139–152.

Lemeille, F., Cushing, M., Carbon, D., Grellet, B., Bitterli, T., Flehoc, C., Innocent, C., 1999a. Co-seismic ruptures and deformations recorded by speleothems in the epicentral zone of the Basel earthquake. Geodinamica Acta 12 (3–4), 179–191.

Lemeille, F., Cushing, M., Cotton, F., Grellet, B., Ménillet, F., Audru, J.C., Renardy, F., Fléhoc, C., 1999b. Traces d'activité pléistocène de failles dans le Nord du fossé du Rhin supérieur (plaine d'Alsace, France). Comptes Rendu de l'Academie des Sciences de Paris 328, 839–846.

Levret, A., Backe, J.C., Cushing, M., 1994. Atlas of macroseismic maps for French earthquakes with their principal characteristics. Natural Hazards 10, 19–46.

Leydecker, G., 1986. Erdbebenkatalog fur die Bundesrepublik Deutschland mit Randgebieten fur die Jahre 1000–1981 (Catalog of earthquakes in the Federal Republic of Germany and adjacent areas from 1000 AD to 1981 AD). Geologisches Jahrbuch, Reihe E: Geophysik 36, 3–83.

Leydecker, G., 2003. Earthquake Catalogue for the Federal Republic of Germany and Adjacent Areas for the Years 800–2002—Datafile, http://www.bgr.de/quakecat—Federal Institute for Geosciences and Natural Resources. Hannover, Germany.

Loew, S., Jenni, J.-P., Blanc, B., 1989. Quantification of surface faulting potential in a low to moderate active region: an example from the Southern Rhinegraben area. Bulletin of the International Association of Engineering Geology 40, 111–116.

López-Ruiz, R., Vázquez-Prada, M., Gómez, J.B., Pacheco, A.F., 2004. A model of characteristic earthquakes and its implications for regional seismicity. Terra Nova 16 (3), 116–120 doi: 10.1111/j.1365-3121.2004.00538.x.

Machette, M., 2000. Active, capable and potentially active faults—a paleoseismic perspective. Journal of Geodynamics 29, 387–392.

Mayer, G., Mai, P.M., Plenefisch, T., Echtler, H., Lüschen, E., Wehrle, V., Müller, B., Bonjer, K.-P., Prodehl, C., Fuchs, K., 1997. The deep crust of the Southern Rhine Graben: reflectivity and seismicity as images of dynamic processes. Tectonophysics 275 (1–3), 15–40.

McClay, K.R., Dooley, T., Whitehouse, P., Mills, M., 2002. 4-D evolution of rift systems: Insights from scaled physical models.

American Association of Petroleum Geologists Bulletin 86 (6), 935–959.

Meghraoui, M., Delouis, B., Ferry, M., Giardini, D., Huggenberger, P., Spottke, I., Granet, M., 2001. Active normal faulting in the upper Rhine Graben and paleoseismic identification of the 1356 basel earthquake. Science 293 (5537), 2070–2073 doi: 10.1126/science.1010618.

Menillet, F., 1995. Les formations superficielles des Vosges et de l'Alsace. Identification, potentialites, contraintes. Bureau des Recherches Gèologiques et Miniéres Rapport Règional 38640, 106pp.

Meyer, B., Lacassin, R., Brulhet, J., Mouroux, B., 1994. The Basel 1356 earthquake: which fault produced it? Terra Nova 6, 54–63.

Miller, S.A., 2002. Earthquake scaling and the strength of seismogenic faults. Geophysical Research Letters 29 (10) 10.1029/2001GL01481.

Musson, R.M.W., 1998. Intensity assignments from historical earthquake data: issues of certainty and quality. Annals of Geophysics 41 (1), 79–91.

Niviére, B., Winter, T., 2001. Pleistocene northward fold propagation of Jura within the southern Upper Rhine Graben: Seismotectonic implications. Global and Planetary Changes 27 (1–4), 263–288.

Niviére, B., Winter, T., Giamboni, M., 2003. Kinematic evolution of a tectonic wedge above a flat-lying decollement: the Alpine foreland at the interface between Jura mountains (N Alps) and south of the Upper Rhine Graben, submitted to Earth Planetary Science Letters, submitted.

Okada, Y., 1985. Surface deformation due to shear and tensile faults in a half-space. Bulletin of the Seismological Society of America 75 (4), 1135–1154.

Okada, Y., 1992. Internal deformation due to shear and tensile faults in a half-space. Bulletin of the Seismological Society of America 82 (2), 1018–1040.

Plenefisch, T., Bonjer, K.-P., 1997. The stress field in the Rhine Graben area inferred from earthquake focal mechanisms and estimation of frictional parameters. Tectonophysics 275 (1), 71–97.

Savage, J.C., Hastie, L.M., 1966. Surface deformation associated with dip-slip faulting. Journal of Geophysical Research 71 (20), 4897–4904.

Schumacher, M.E., 2002. Upper Rhine Graben: Role of preexisting structures during rift evolution. Tectonics 21 (1), 1006 10.1029/2001TC900022.

Schwartz, D.P., Coppersmith, K.J., 1984. Fault behavior and characteristic earthquakes: examples from the Wasatch and San Andreas fault zones. Journal of Geophysical Research 89, 5681–5698.

Shebalin, N.V., 1973. Macroseismic data as information on source parameters of large earthquakes. Physics of the Earth and Planetary Interiors 6, 316–323.

Sieberg, A., 1940. Beiträge zum Erdbebenkatalog Deutschlands und angrenzender Gebiete für die Jahre 58 bis 1799. Mitteilungen des Deutschen Reichs-Erdbebendienstes, 2.

SISFRANCE, 2004, Histoire et caractéristiques des séismes ressentis en France métropolitaine et sur ses abords, BRGM (Bureau de Recherches Geologiques et Minieres), EDF (Electricitè de France) and IRSN (Institut de Radioprotection et Sureté Nucleaire). http://www.sisfrace.net.

Sissingh, W., 1998. Comparative Tertiary stratigraphy of the Rhine Graben, Bresse Graben and Molasse Basin: correlation of Alpine foreland events. Tectonophysics 300 (1–4), 249–284.

Sponheuer, W., 1960. Methoden zur Herdtiefenbestimmung in der Makroseismik. Freiburg Forschung-Hoschule 88, 117pp.

Stirling, M., Rhoades, D., Berryman, K., 2002. Comparison of Earthquake Scaling Relations Derived from Data of the Instrumental and Preinstrumental Era. Bulletin of the Seismological Society of America 92 (2), 812–830.

Valensise, G., Pantosti, D., 2001a. The investigation of potential earthquake sources in peninsular Italy: a review. Journal of Seismology 5, 287–306.

Valensise, G., Pantosti, D. (Eds.), 2001b. Database of Potential Sources for Earthquakes Larger than M 5.5 in Italy. Annali di Geofisica 44, Supplemento 1, with CD-ROM.

Valensise, G., Basili, R., Mucciarelli, M., Pantosti, D. (Eds.), 2002. Database of Potential Sources for Earthquakes Larger than M 5.5 in Europe, a compilation of data collected by partners of the EU project FAUST. http://www.ingv.it/~roma/banche/catalogo_europeo.

Vogt, H., 1991. Neotectonics and geomorphological evolution on the Southwestern border of the Rhinegraben. Zeitschrift für Geomorphologie Neue Folge Supplement-Band 82, 35–45.

Wells, D.L., Coppersmith, K.J., 1994. New empirical relationships among magnitude, rupture length, rupture width, rupture area, and surface displacement. Bulletin of the Seismological Society of America 84, 974–1002.

Winter, T., Niviére, B., Lambert, J., 2002. Seismotectonic Model for the Southern Upper Rhine Graben-Deliverable 4.1. 5PCRD SAFE Project Report.

Ziegler, P.A., 1992. European Cenozoic rift systems. Tectonophysics 208, 91–111.